Tumor evolution of glioma intrinsic gene expression subtype associates with immunological changes in the microenvironment

Qianghu Wang[1, 2, 3*], Xin Hu[1, 8*], Baoli Hu[4], Florian Muller[1, 5], Hoon Kim[1], Massimo Squatrito[9], Tom Mikkelsen[10], Lisa Scarpace[10], Floris Barthel[11], Yu-Hsi Lin[5], Nikunj Satani[5], Emmanuel Martinez-Ledesma[1], Edward Chang[1], Adriana Olar[6], Guocan Wang[4], Ana C. deCarvalho[10], Eskil Eskilsson[1], Siyuan Zheng[1], Amy B. Heimberger[7], Erik P. Sulman[2†], Do-Hyun Nam[12, 13, 14†], Roel G.W. Verhaak[1, 3†]

[1]Department of Genomic Medicine, [2]Department of Radiation Oncology, [3]Department of Bioinformatics and Computational Biology, [4]Department of Cancer Biology, [5]Department of Cancer Systems Imaging, [6]Department of Pathology, [7]Department of Neurosurgery, The University of Texas MD Anderson Cancer Center, Houston, TX 77030, USA; [8]University of Texas-Houston Graduate School in Biomedical Sciences, Houston, TX 77030, USA; [9]Cancer Cell Biology Programme, Seve Ballesteros Foundation Brain Tumor Group, Centro Nacional de Investigaciones Oncológicas, CNIO, 28029 Madrid, Spain; [10]Departments of Neurology and Neurosurgery, Henry Ford Hospital, Detroit, MI 48202, USA; [11]Oncology Graduate School Amsterdam, VU University Medical Center, 1081 HV Amsterdam, The Netherlands; [12]Institute for Refractory Cancer Research, Samsung Medical Center, Seoul 06351, Korea; [13]Department of Health Sciences and Technology, Samsung Advanced Institute for Health Sciences and Technology, Sungkyunkwan University, Seoul 06351, Korea; [14]Department of Neurosurgery Samsung Medical Center, Sungkyunkwan University School of Medicine, Seoul, 135-710, Korea.

* These authors contributed equally
[†]Co-senior authors

Correspondence: epsulman@mdanderson.org, nsnam@skku.edu, rverhaak@mdanderson.org

Keywords: glioblastoma, disease recurrence, mesenchymal subtype, proneural to mesenchymal transition, gene expression profiling, tumor microenvironment, macrophages/microglia, immune cells.

Summary

We leveraged IDH wild type glioblastomas and derivative neurospheres to define tumor-intrinsic transcription phenotypes. Transcriptomic multiplicity correlated with increased intratumoral heterogeneity and tumor microenvironment presence. In silico cell sorting demonstrated that M2 macrophages/microglia are the most frequent type of immune cells in the glioma microenvironment, followed by CD4 T lymphocytes and neutrophils. Hypermutation associated with CD8+ T cell enrichment. Longitudinal transcriptome analysis of 124 pairs of primary and recurrent gliomas showed expression subtype is retained in 53% of cases with no proneural to mesenchymal transition being apparent. Inference of the tumor microenvironment through gene signatures revealed a decrease in invading monocytes but a subtype dependent increase in M2 macrophages/microglia cells after disease recurrence. All expression datasets are accessible through http://recur.bioinfo.cnio.es/.

Significance

IDH wild type glioblastoma expression phenotypes have been related to tumor characteristics including genomic abnormalities and treatment response. We explored the intratumoral transcriptomic landscape, including a definition of tumor-intrinsic gene expression subtypes and how they relate to the different cellular components of the tumor immune environment. Comparison of matching primary and recurrent gliomas provided insights into the treatment-induced phenotypic tumor evolution. Proneural to mesenchymal transitions have long been suspected but were not apparent, while intratumoral heterogeneity was a predictor of subtype transition upon recurrence. Characterizing the evolving glioblastoma transcriptome en tumor microenvironment aids

54   in designing more effective immunotherapy trials. Our study provides a comprehensive

55   transcriptional and cellular landscape of IDH wild type GBM during treatment modulated

56   tumor evolution.

57

58   **Highlights**

59   • Next generation GBM-intrinsic transcriptional subtypes: proneural, classical,

60   mesenchymal

61   • M2 macrophages, CD4+ T-lymphocytes and neutrophils dominate glioblastoma

62   microenvironment

63   • Sensitivity to radiotherapy may associate with M2 macrophage presence

64   • CD8+ T cells are enriched in hypermutated GBMs at diagnosis and recurrence

INTRODUCTION

The intrinsic capacity of glioblastoma (GBM) tumor cells to infiltrate normal brain impedes surgical eradication and predictably results in high rates of early recurrence. To better understand determinants of GBM tumor evolution and treatment resistance, The Cancer Genome Atlas Consortium (TCGA) performed high dimensional profiling and molecular classification of nearly 600 GBM tumors (Brennan et al., 2013; Cancer Genome Atlas Research, 2008; Ceccarelli et al., 2016; Noushmehr et al., 2010; Verhaak et al., 2010b). In addition to revealing common mutations in genes such as *TP53*, *EGFR*, *IDH1*, and *PTEN*, as well as the frequent and concurrent presence of abnormalities in the p53, RB and receptor tyrosine kinase pathways. Unsupervised transcriptome analysis identified four clusters, referred to as classical, mesenchymal, neural and proneural, that were tightly associated with genomic abnormalities(Verhaak et al., 2010a). The proneural and the mesenchymal expression subtypes have been most consistently described in literature with proneural relating to a more favorable outcome and mesenchymal to unfavorable survival (Huse et al., 2011; Phillips et al., 2006; Zheng et al., 2012), but these findings were affected by the relatively favorable outcome of IDH-mutant glioblastoma which are consistently classified as proneural (Noushmehr et al., 2010; Verhaak et al., 2010a). Proneural to mesenchymal switching upon disease recurrence has been described as a source for treatment resistance in GBM relapse (Bao et al., 2006; Bhat et al., 2013; Ozawa et al., 2014; Phillips et al., 2006), but the relevance of this phenomenon in glioma progress remains ambiguous.

GBM tumor cells along with the tumor microenvironment create a complex milieu that ultimately promotes tumor cell plasticity and disease progression (Olar and Aldape,

88 2014). The presence of tumor-associated stroma results in a mesenchymal tumor gene

89 signature and poor prognosis in colon cancers (Isella et al., 2015). Furthermore, the

90 association between a mesenchymal gene expression signature and reduced tumor

91 purity has been identified as a common theme across cancer (Martinez et al., 2015;

92 Yoshihara et al., 2013). Tumor-associated macrophages/microglia in GBM have been

93 proposed as regulators of proneural-to-mesenchymal transition through NF-kB

94 activation (Bhat et al., 2013) and may provide growth factor mediated proliferative

95 signals, which could be therapeutically targeted (Patel et al., 2014; Pyonteck et al.,

96 2013; Yan et al., 2015).

97   Here, we explored the properties of the microenvironment in different GBM gene

98 expression subtypes and characterized the transition between molecular subtypes

99 before and after therapeutic intervention. In doing so, we improved the robustness of

100 gene expression subtype classification through revised gene signatures and proposed

101 analytical methodology. Our results suggested that the tumor microenvironment

102 interferes with expression based classification of GBM, both at the primary disease

103 stage as well as at disease recurrence, and suggest a role for the

104 macrophage/microglia in treatment response.

105 **RESULTS**

106 ***Harnessing glioma sphere-forming cells identifies GBM specific intertumoral***

107 ***transcriptional heterogeneity***

108 We set out to elucidate the tumor-intrinsic and tumor microenvironment independent

109 transcriptional heterogeneity of GBMs. We performed a pairwise gene expression

110 comparison of independent set of GBMs and the derivative glioma sphere-forming cells

111 (GSCs) (n = 37) (Galli et al., 2004). In total, 5,334 genes were found to be significantly

112 higher expressed in parental GBMs relative to derived GSCs that could be attributed by

113 the tumor associated GBM microenvironment (**Figure 1A**). To focus the analysis on the

114 tumor-intrinsic transcriptome, these genes were filtered from further analysis. GBMs

115 with IDH mutations have distinct biological properties and favorable clinical outcomes

116 compared to IDH wild-type GBMs (Brennan et al., 2013; Cancer Genome Atlas

117 Research et al., 2015; Ceccarelli et al., 2016; Noushmehr et al., 2010). Using the

118 filtered gene set, we performed consensus non-negative matrix factorization clustering

119 to identify three distinct subgroups amongst 369 IDH wild type GBMs (**Figure 1B;**

120 **Figure 1C**). When comparing the clustering result with the previously defined proneural

121 (PN), neural (NE), classical (CL) and mesenchymal (MES) classification (Brennan et al.,

122 2013; Verhaak et al., 2010b), three subgroups were strongly enriched for CL, MES and

123 PN GBMs, respectively (**Figure S1**). Consequently, we labeled the groups as CL, MES

124 and PN. None of the three subgroups was enriched for the NE class, suggesting its

125 neural phenotype is non-tumor specific. The NE group has previously been related to

126 the tumor margin where normal neural tissue is more likely to be present (Gill et al.,

127 2014; Sturm et al., 2012) and such contamination might explain why the neural subtype

6

128   was the only subtype to lack characteristic gene abnormalities (Brennan et al., 2013;

129   Verhaak et al., 2013). To be able to classify external GBM samples, we implemented a

130   single sample gene set enrichment analysis (ssGSEA) based equivalent distribution

131   resampling classification strategy using 70-gene signatures for each subgroup (**Table**

132   **S1**)(**Figure 1D**), to assign each sample three empirical classification p-values by which

133   we determined the significantly activated subtype(s) in the samples. We prepared an R-

134   library to facilitate others to evaluate our approach (Supplementary File 1). Using this

135   method we found that the stability of cluster assignments of 144 TCGA GBM samples

136   profiled using both RNA sequencing and Affymetrix U133A microarrays was 95%

137   concordance (**Figure S2, Table S2**). This was an improvement over the 77% subtype

138   concordance determined using previously reported methods (Verhaak et al., 2010b).

139   We evaluated the distribution of somatic variants across all the three molecular

140   subtypes (**Figure 1E)(Figure S3)** and confirmed the strong associations between

141   subtypes and genomic abnormalities in previously reported driver genes (Brennan et al.,

142   2013; Verhaak et al., 2010b).

143

144   ***Multi-activation of subtype signatures associated with intratumoral heterogeneity***

145   We observed that 34/369 (9.2%) samples showed significant enrichment of multiple

146   ssGSEA scores (empirical classification p-value<0.05), suggesting these cases activate

147   more than one transcriptional subtype (**Figure 2A**). To quantify this phenomenon, a

148   score ranging from 0 to 1 was defined to quantitatively evaluate the simplicity of subtype

149   activation based on order statistics of ssGSEA score. Samples with high simplicity

150   scores activated a single subtype and those with lowest simplicity scores activated

151 multiple subtypes. All multi-subtype TCGA samples showed simplicity scores of less

152 than 0.1 (**Figure 2A**). To determine whether transcriptional heterogeneity associated

153 with genomic intratumoral heterogeneity, we correlated simplicity scores, total mutation

154 rates and subclonal mutation rates. Included in the analysis were 224 TCGA GBMs with

155 available whole exome sequencing data (Kim et al., 2015) and ABSOLUTE (Carter et

156 al., 2012) determined high tumor purity (> 0.8) to equalize the mutation detection

157 sensitivity (Aran et al., 2015). Although not significant (Wilcoxon rank test p-

158 value=0.143), the total mutation rate was less in the bottom 30% with lowest simplicity

159 scores versus the top 30% samples with highest simplicity scores. The subclonal

160 mutation rate was significantly higher (p-value=0.024) in samples with lowest simplicity

161 scores (**Figure 2B; Table S3**), suggesting that increased intratumoral heterogeneity

162 associates with increased transcriptional heterogeneity.

163 We compared outcomes amongst the three transcriptional groups and observed

164 no significant differences (**Figure S4**). However, when restricting the analysis to

165 samples with high simplicity scores, a clear trend of MES showing worst survival and

166 PN the most favorable outcome became visible. For example, Kaplan-Meier analysis of

167 88 samples with simplicity scores >0.99 showed a median survival of 11.4, 14.7 and

168 16.7 months were detected in MES, CL and PN, respectively, which was significantly

169 different (log rank test, p=0.048)(**Figure 2C)(Figure S4)(Table S4**). Higher simplicity

170 scores correlated with relative favorable outcome within the PN set, non-significant in

171 the CL subtype, and correlated with relatively unfavorable survival in the MES class

172 (**Figure S5**).

8

173   Single GBM cell RNA sequencing recently suggested that GBMs are comprised

174   of a mixture of tumor cells with variable GBM subtype footprints (Patel et al., 2014). We

175   used this data to classify 502 single GBM cells in addition to the bulk tumor derived from

176   five primary glioblastomas (**Table S5**). All bulk tumor samples showed simplicity scores

177   less than 0.05 suggesting high transcriptional heterogeneity compared to 45 of 369

178   TCGA GBM samples with simplicity scores below 0.05 (**Figure 2D**). In four of five cases

179   (MGH26, MGH28, MGH29 and MGH30), the bulk tumor samples were classified in the

180   same primary subtype as the majority of their single cells (**Figure 2D**). Our analysis

181   suggests that the heterogeneity observed at the single cell level is captured in the

182   expression profile of the bulk tumor, and that the five GBM samples studied at the single

183   cell level represented samples with relatively high transcriptional heterogeneity.

184

185   ***Transcriptional subtypes differentially activate the immune microenvironment***

186   Despite restricting the cluster analysis to genes exclusively expressed by GBM cells, we

187   found that tumor purity predictions based on ABSOLUTE were significantly reduced in

188   GBM classified as MES (Student T-test p-value < 10e-14; **Figure 3A**). This was

189   corroborated by gene expression based predictions of tumor purity using the

190   ESTIMATE method (Student T-test p-value < 10e-32; **Figure 3B**)(Yoshihara et al.,

191   2013) . The ESTIMATE method has been optimized to quantify tumor-associated

192   fibroblasts and immune cells (Yoshihara et al., 2013) and the convergence of a

193   decreased ABSOLUTE and decreased ESTIMATE tumor purity confirmed previous

194   suggestions on the increased presence of microglial and neuroglial cells mesenchymal

195   GBM (Bao et al., 2006; Engler et al., 2012; Gabrusiewicz et al., 2016; Ye et al., 2012).

196   The mean simplicity score of samples classified as MES was 0.53 which was

197   significantly lower than in PN (Wilcoxon rank test p-value<0.019) and CL subtypes

198   (Wilcoxon rank test p-value<0.0001), confirming increased transcriptional heterogeneity.

199   In order to identify genomic determinants of macrophage/microglia chemoattraction, we

200   compared genomic alterations between mesenchymal class samples with high (n=51)

201   and low (n=51) ABSOLUTE based tumor purity. GBM carrying hemyzygous loss of *NF1*

202   or somatic mutations in *NF1* showed reduced tumor purity compared to GBM with wild

203   type *NF1* (Wilcoxon rank test p-value=0.0007) and this association was similarly

204   detected when limiting the analysis to MES samples (Wilcoxon rank test p-

205   value=0.017)(Figure S6). Formation of dermal neurofibromas in the context of *Nf1* loss

206   of heterozygosity has been reported to be context and microenvironment dependent (Le

207   et al., 2009). Functional studies may clarify whether NF1 deficient GBM are able to

208   recruit cells that provide them with a proliferative advantage, or whether *NF1* loss

209   provides that proliferative advantage in a specific tumor-associated microenvironment

210   context.

211   To determine the cellular components of the tumor microenvironment across

212   different transcriptional subtypes, we used the CIBERSORT in silico cytometry

213   (Newman et al., 2015) method to evaluate absolute immune cell fractions. We

214   evaluated 22 different immune cell types in 69 PN, 137 CL and 96 MES samples, after

215   filtering samples with classification simplicity scores less than 0.1 (**Table S6**). Microglia

216   are the resident macrophages in the central nervous system. Peripheral blood

217   monocytes also give rise to tumor associated macrophages. These innate immune cells

218   can be broadly classified as the proinflammatory M1 type and the alternative tumor

219   promoting M2 type(Hambardzumyan et al., 2015). The M2 macrophage gene signature

220   showed a greater association with the MES subtype (13.4%) relative to the PN (4.6%)

221   and CL (6.0%)(**Figure 3C**), consistent with previous analysis of the TCGA

222   database(Doucette et al., 2013; Gabrusiewicz et al., 2016). In addition to the M2

223   macrophage gene signature, there was also a significantly higher fraction of MES

224   samples that expressed M1 macrophage (Student T-test p-value 3.20E-5) and

225   neutrophil (Student T-test p-value 1.30E-9) gene signatures. In contrast, the activated

226   natural killer T-cell gene signature (Student T-test p-value 4.91E-2) was significantly

227   reduced in the MES subtype and resting memory CD4+ T cells (Student T-test p-value

228   5.40E-7) were less frequently expressed in the PN subtype.

229   To confirm the association of macrophages/microglia with the MES GBM subtype,

230   we assessed protein expression levels of the ITGAM (alternatively known as CD11B)

231   and IBA1 (also known as AIF1) macrophage/microglial markers in a set of 18 GBM for

232   which we also characterized the expression subtype (**Figure 3D**) as well as through

233   immunohistochemistry (**Figure S7**). We confirmed the microenvironment as the main

234   source for *ITGAM/IBA1* transcription by comparing transcriptional levels in 37 GBM-

235   neurosphere pairs used for gene filtering, which showed that neurospheres do not

236   express *ITGAM/IBA1* (**Figure 3E**). The association of the MES GBM subtype with

237   increased level of M2 microglia/macrophages may suggest that in particular MES GBM

238   are candidates for therapies directed against tumor-associated macrophages(Pyonteck

239   et al., 2013). Activated dendritic cell signatures (Student T-test p-value 7.36E-3)(**Figure**

240   **3C**) were significantly higher in the CL subtype, suggesting this subtype may benefit

241   from dendritic cell vaccines (Palucka and Banchereau, 2012). Dendritic cells may

242   require an activated phenotype in order to direct the immune system. A previous study

243   suggested that MES GBM patients treated with dendritic cells were more likely to

244   benefit (Prins et al., 2011).

245

246   ***Phenotypic plasticity upon GBM recurrence***

247   Glioblastoma has long been hypothesized to progress along a proneural to

248   mesenchymal axis(Phillips et al., 2006). To determine the relevance of this transition

249   process in IDH wildtype glioma evolution, we performed a longitudinal analysis of the

250   subtype classification and tumor-associated microenvironment in sample pairs obtained

251   at diagnosis and first disease recurrence from 124 glioma patients. The cohort included

252   96 initial GBM and first recurrence, eight pairs of primary low grade glioma and

253   matching secondary GBM, and 20 pairs of primary and recurrent low grade glioma.

254   Gene expression profiles of 78 tumor pairs were analyzed through transcriptome

255   sequencing, and remaining pairs were generated using Affymetrix (n = 31) and Illumina

256   (n = 15) microarray, respectively. To facilitate exploration of this dataset we have made

257   it available through the GlioVis portal http://recur.bioinfo.cnio.es/. We used a gene

258   expression signature(Baysan et al., 2012) to determine that 33 of 124 cases were IDH-

259   mutant/GCIMP at presentation and recurrence (**Table S7**). We used the renewed gene

260   signatures and classification method to determine molecular subtype of the 91 pairs of

261   IDH wild type cases and found that expression class remained consistent after disease

262   recurrence for 48 of 91 IDH-wildtype cases (52%)(**Figure 4A**). The MES subtype was

263   most stable (64%) while the CL (47%) and PN (43%) phenotypes were less frequently

264   retained. Nine, sixteen and eighteen post-treatment tumors switched subtypes to

12

265 become CL, MES and PN at disease recurrence, respectively, indicating that PN and

266 MES increased in frequency after recurrence while the CL subtype was least frequently

267 found (**Figure 4A**). The CL expression class was previously found to be most sensitive

268 to intensive therapy and it is possible that therapy provides a competitive advantage for

269 non-CL cells, which could explain the reduced post-treatment incidence(Verhaak et al.,

270 2010b). Our results did not identify enrichment for proneural to mesenchymal transitions.

271 We observed a significant difference in transcriptional simplicity between primary

272 GBM retaining their expression class, versus those that switched to a different

273 phenotype (**Figure 4B**). GBMs with a primary tumor simplicity score greater than 0.5,

274 indicated lower transcriptional heterogeneity, were classified as the same subtype in 31

275 of 48 (64.5%) cases, compared to 15 of 41 (36.6%) cases with primary tumor simplicity

276 scores less than 0.5 (Fisher exact test p-value=0.01).

277

278 ***Microenvironment transitions upon GBM recurrence***

279 Debulking surgery, radiotherapy and chemotherapy provide therapeutic barriers but

280 nonetheless induce tumor evolution, including influences on the tumor

281 microenvironment. We explored this possibility by comparing the tumor associated

282 microenvironment in primary and recurrent GBMs using CIBERSORT (**Table**

283 **S8**)(Newman et al., 2015). A comparison between 91 primary and recurrent IDH-wild

284 type tumors revealed a decrease in monocyte gene signature expression at recurrence,

285 suggesting relative depletion of circulation derived monocytes (**Figure 5A**). Next, we

286 dissected microenvironment fluctuations between diagnosis and recurrent tumors

287 across different subtype combinations. Primary non-MES (CL or PN) tumors showed

13

288   relatively high tumor purity and consequently, recurrent tumors classified as non-MES

289   demonstrated a relatively global decrease of immune cells while cases transitioning to

290   MES at recurrence represented a trend towards increased immune cell fractions

291   (**Figure 5B**). Gene signatures of immunosuppressive regulatory T cells showed an

292   increase in gene expression at recurrence across several primary-recurrence subtype

293   combinations although the inferred cellular fractions are relatively small (**Figure 5B**). In

294   contrast to the trend of monocyte depletion, the imputed M2 macrophage frequency was

295   significantly higher at recurrence in cases transitioning to MES (**Figure 5C**). This

296   observation converges with the higher predicted fraction of M2 macrophages in primary

297   MES GBM relative to primary non-MES GBM. M1 macrophages and neutrophils also

298   correlated with primary MES GBM, but these associations were not confirmed for

299   recurrent GBM. We validated the increase in macrophages using immunostaining of

300   IBA1 expression in two primary-recurrent GBM pairs which were classified as CL to

301   MES (**Figure 5D**). IBA1 immunoexpression was restricted to macrophages/microglia,

302   cells exhibiting either globular or filamentous/spidery morphology, with no expression in

303   glioma tumor cells (**Figure 5D**). Quantitative analysis of microglia frequency using

304   Inform software for automated pathology imaging processing confirmed a significantly

305   higher presence (p value = 2.25e-11 and 2.12e-13 for patient #1 and #2, respectively) of

306   at MES recurrence (**Figure 5E**). These findings further solidify the association between

307   MES GBM and macrophage/microglia and extend this mutual relationship to disease

308   recurrence. MES tumors at recurrence compared to primary MES tumors showed an

309   increase in transcriptional activity associated with non-polarized M0 macrophages,

310   which has been previously described (Gabrusiewicz et al., 2016), but also dendritic cells

14

311 which is potentially motivated by the increased levels of neoantigens at disease

312 recurrence (Kim et al., 2015). In contrast, primary PN GBM were found to contain

313 significantly higher fractions of five immune cell categories compared to recurrent PN

314 GBM, indicating a relative absence of immune infiltration in PN GBM upon recurrence.

315 We evaluated the effect of transcriptional class on patient survival. The analysis

316 was restricted to 50 cases for whom annotation on overall survival (OS) time and time to

317 disease progression (PFS) were available and with high simplicity scores, indicating low

318 transcriptional heterogeneity. We confirmed the worse prognosis for patients whose

319 primary tumor was classified as MES on overall survival (logrank test p=0.029 with

320 HR=1.97)(**Figure 6A; Figure 6B**). This pattern was retained in patients whose

321 secondary glioma was classified as MES (logrank test p=0.09 with HR=1.71)(**Figure 6C;**

322 **Figure 6D**). Consequently, cases for whom both primary and recurrent tumor were

323 classified as MES subtype showed the least favorable outcome, suggesting an additive

324 effect of transcriptional class at different time points (**Figure 6E, Figure 6F**)(**Figure S8**).

325

326 ***Treatment-Induced Immunological Microenvironment Changes upon GBM***

327 ***recurrence***

328 Temozolomide treatment of gliomas can induce hypermutation(Hunter et al., 2006; Kim

329 et al., 2015). Missense mutations may generate neoantigens that can be recognized

330 which by CD8+ T lymphocytes (Schumacher and Schreiber, 2015). Using matching

331 exome data we classified five recurrent gliomas in our dataset as being hypermutated at

332 (>=400 SNVs). The predicted frequency of CD8+ T cells was significantly increased at

333 recurrence in comparison to their primary tumors (median 7.7‰ vs 1.9‰; Wilcoxon rank

15

334   test p-value=0.008)(**Figure 7A**). This observation was further validated by comparing

335   seven hypermutated primary GBMs to 238 non-hypermutated GBMs (median 7.0‰ vs

336   0‰; Wilcoxon rank test p-value=0.031)(**Figure 7B**). The majority (61%) of non-

337   hypermutated primary GBMs showed predicted CD8+ T cell fractions equal to zero. The

338   observation suggests that patients with hypermutated tumors are more likely to benefit

339   from CD8+ T cell antitumor immunity.

340   Preclinical studies suggested radiation may increase the recruitment of T cells in

341   the tumor microenvironment (Deng et al., 2014; Zeng et al., 2013). We compared the

342   microenvironment of primary GBM treated with radiation therapy and separated short

343   term relapse (PFS > 6 months, n = 27) from late relapse (PFS > 12 months, n = 21).

344   Evaluating the gene signature based presence of M2 macrophages and CD4+ T cells

345   (CD4+ T memory resting and CD4+ follicular helper cells) in 75 IDHwt GBM pairs whom

346   received radiotherapy, we observed no significant difference between primary tumors

347   with short-term and long-term relapse but found a significant increase after radiation at

348   recurrence (**Figure 7C, D, E**). M2 macrophages have been speculated to play a role in

349   resistance to radiotherapy(Meng et al., 2010; Ruffell and Coussens, 2015) and

350   macrophage targeting immunotherapy (Pyonteck et al., 2013; Ries et al., 2014) may

351   play a radiosensitizing role. The increasing of CD4+ T cells at recurrence for short term

352   relapse tumors points towards inhibiting CTLA-4 as adjuvant therapy to radiation.

353

16

DISCUSSION

354

355 Transcriptome profiling of tumor samples is a commonly used modality for interrogating

356 pathway functionality and phenotype based patient classification. The transcriptional

357 footprint left by the tumor microenvironment, which may constitute 10-80% of cells in a

358 tumor biopsy(Yoshihara et al., 2013), can obscure the true activity of the signaling

359 network(Isella et al., 2015; Kim and Verhaak, 2015). Here, we employed in silico

360 methods to integrate mRNA expression profiles from glioma samples and glioma cell

361 culture models to provide insights into glioma-intrinsic pathway activities and

362 classification, and to deconvolute the glioma associated stroma into its immunological

363 cellular components.

364 GBM expression subtype classification has emerged as an important concept to

365 better understand the biology of this devastating disease (Dunn et al., 2012; Huse et al.,

366 2011; Sturm et al., 2014). Robust classification of new GBM tumors is therefore critical

367 to ensure consistency in reporting between different studies. The transcriptional glioma

368 subtypes we discovered using tumor-intrinsic gene expression values strongly

369 overlapped with the proneural, classical and mesenchymal subtypes but identified the

370 neural class as normal neural lineage contamination. Our updated methods, released

371 through a R-library, were found to be highly robust and provide the community with a

372 standardized strategy for classification of gliomas.

373 Through re-classification of primary GBM samples from TCGA and despite using

374 tumor-only transcripts, we observed that the mesenchymal GBM subtype associated

375 with the presence of tumor-associated glial and microglial cells. Mesenchymal glioma

376 cell differentiation status has been found to correlate with enrichment of

377   macrophages/microglia (Bhat et al., 2013; Kreutzberg, 1996). Through in silico cell type

378   identification we additionally detected enrichment of various adaptive immunity cell

379   types, including CD4+ T lymphocytes.

380   Longitudinal analysis of tumor samples is complicated by the lack of tissue

381   collections including such pairs. Through aggregation of existing and novel datasets we

382   compiled a cohort of 124 glioma pairs, including 91 pairs of IDH wild type tumors.

383   Comparison of pairs of initial gliomas and first disease recurrence did not identify the

384   trend of proneural GBM transitioning to a mesenchymal phenotype that has often been

385   suspected (Phillips et al., 2006). Mesenchymal subtype at diagnosis and at disease

386   recurrent correlated with relatively poor outcome. The recurrent IDH wild type GBM

387   immuno environment showed fewer blood derived monocytes which may reflect lower

388   penetration through the blood brain barrier. While the frequency of M2

389   macrophage/microglia was increased in recurrent mesenchymal GBM compared to

390   primary non-mesenchymal GBM, the overall fraction of M2 macropage/microglia

391   remained stable. This possibly suggests that the majority of these cells are derived from

392   resident CNS macrophages than through active recruitment from the circulation.

393   In summary, our study defines a new strategy to determine transcriptional

394   subtype, and associated expression classes to the tumor-associated immuno-

395   environment. Our findings may aid in the implementation of immunotherapy approaches

396   (Blank et al., 2016) in a disease type with very limited treatment options. Collectively,

397   our results have improved our understanding of determinants of GBM subtype

398   classification, the critical impact of the tumor microenvironment, and provide new

399   handles on the interpretation of transcriptional profiling of glioma.

18

EXPERIMENTAL PROCEDURES

Collection of pairs of primary and recurrent glioma samples

U133A array profiles for 543 primary GBM, and RNA-Seq data for 166 primary and 13 recurrent GBM were obtained from the TCGA portal https://tcga-data.nci.nih.gov/tcga/. Mutation calls and DNA copy number profiles were obtained for all samples, where available. Tissues from 20 additional initial GBM and matched recurrent tumor were obtained from Henry Ford Hospital (n = 9) in accordance with institutional policies and all patients provided written consent, with approval from the Institutional Review Boards (Henry Ford Hospital IRB protocol #402). All RNA samples tested were obtained from frozen specimens. All of the recurrent GBMs had been previously treated with chemotherapy and radiation. Three cases had a history of lower grade astrocytoma prior to the first GBM (HF-2869/HF-3081/HF-3162). Tumors were selected solely on the basis of availability. RNA-Seq libraries were generated using RNA Truseq reagents (Illumina, San Diego, CA, USA) and paired-end sequenced using standard Illumina protocols. Read length was 76 base pairs for cases sequenced by TCGA and from Henry Ford (processed at MD Anderson). RNA-Seq data on frozen tissue from 44 patients with initial and recurrent GBM that received resection at Samsung Medical Center and Seoul National University Hospital were provided by Dr. Nam's lab. Surgery specimens were obtained in accordance to the Institutional Review Board (IRB) of the Samsung Medical Center (No. 2010-04-004) and Seoul National University Hospital (No. C-1404-056-572). Affymetrix CEL files of 39 pairs of initial and recurrent glioma were retrieved from the Gene Expression Omnibus (GEO accession GSE4271, GSE42670, GSE62153)(Joo et al., 2013; Kwon et al., 2015; Phillips et al., 2006). The expression

19

423 profiles of the 23 pairs from GSE4271 were determined using Affymetrix HG-U133

424 GeneChips, the 1 pairs from GSE42670 were analyzed using the Affmetrix HuGene-1-

425 0-st platform, the 15 pairs from GSE62153 were analyzed using Illumina Human HT-12

426 V4.0 expression BeadChip. The RNA sequencing data of 14 and 5 pairs of primary and

427 recurrent low grade glioma were from TCGA LGG cohort and

428 EGAS00001001255(Mazor et al., 2015), respectively.

429   Genome wide DNA copy number profiling and exome sequencing on thirteen

430 TCGA tumor pairs and nine of ten Henry Ford tumor pairs were performed and data

431 was analyzed using standard protocols and pipelines as previously described (Kim et al.,

432 2015).

433

434 ***Data for multiplatform classification comparison***

435 RNA sequencing data was available for 162 primary GBMs(Brennan et al., 2013) for

436 which an Affymetrix HT-U133A gene expression profile was also available. We

437 observed a low Pearson Correlation Coefficient (< 0.15) between RNA sequencing

438 based reads per kilo base of transcript per million reads (RPKM) and Affymetrix HT-

439 U133A profiles in eighteen cases and these were removed from further analysis. In

440 summary, in order to assess the concordance between classification results of the new

441 70-gene signatures and previously published 210-gene signatures (Verhaak et al.,

442 2010b), 144 GBMs which were profiled in both RNA sequencing and Affymetrix U133A

443 platforms were used in our further analyses.

444

445 ***Transcriptome Data processing***

20

446 The latest version custom CDF files (Version19, http://brainarray.mbni.med.umich.edu)

447 (Dai et al., 2005; Sandberg and Larsson, 2007) were used to map probes from the

448 Affymetrix HG-U133A and HuGene-1_0-st GeneChip platforms to the Ensemble

449 transcript database, combined in one probe set per gene and normalized using the

450 AROMA package with default parameters, resulting in RMA normalized and log

451 transformed gene expression values (Bengtsson et al., 2009). All RNA sequencing data

452 was processed by the PRADA pipeline (Torres-Garcia et al., 2014). Briefly, reads were

453 aligned using BWA against the genome and transcriptome. After initial mapping, the

454 aligned reads were filtered out if their best placements are only mapped to unique

455 genomic coordinates. Quality scores are recalibrated using the Genome Analysis

456 Toolkit (GATK), and duplicate reads are flagged using Picard. Mapped features were

457 quantified and normalized per kilo base of transcript per million reads (RPKM) and were

458 converted to a log2 scale to represent a gene expression level. RPKM values

459 measuring the same gene that mapped to the Ensemble transcript with longest size

460 were selected to obtain one expression value per gene and sample. RPKM values were

461 converted to a log2 scale to represent gene expression level. The statistical

462 environment R was used to perform all the statistical analysis and graph plots.

463

464 ***Deriving new gene signatures***

465 A pair-wise gene expression analysis identified 5,334 genes which are significant higher

466 expressed in glioma bulk samples compared to their derivative GSCs. These genes

467 were discarded from the gene list for developing tumor-specific molecular subtypes.

468 Consensus non-negative matrix factorization (CNMF) clustering method identified three

469 distinct subgroups among the 369 IDHwt primary GBMs. A set of 270 GBMs was

470 recognized as core samples based on a positive silhouette width. The gene expression

471 values of each subtype were compared with those from the other two subtypes

472 combined (Verhaak et al., 2010b). Signature genes per cluster were selected on the

473 basis of differences in gene expression level and were considered significant if they

474 reached the cut-off value with t-test p-value< 1E-3 for higher expressed in this class,

475 while also showing a significant lower expression with t-test p-value<1E-3 in the other

476 two classes. In the original gene signatures, genes could be either down-regulated or

477 up-regulated, while only up-regulated genes (n=70 per gene signature) were selected

478 for revised gene signatures. Only genes measured on both RNAseq and U133A

479 platforms were considered, and the U133A data from 162 GBM samples measured on

480 both platforms (which included the 144 cases used to compare U133A and RNAseq

481 results) was used in the final comparative analysis.

482

483 ***Molecular classifications based on ssGSEA enrichment scores***

484 Single sample gene set enrichment analysis was performed as follows. For a given

485 GBM sample, gene expression values were rank-normalized and rank-ordered. The

486 Empirical Cumulative Distribution Functions (ECDF) of the signature genes and the

487 remaining genes were calculated. A statistic was calculated by integration of the

488 difference between the ECDFs, which is similar to the one used in GSEA but is based

489 on absolute expression rather than differential expression (Barbie et al., 2009). Since

490 the ssGSEA test is based on the ranking of genes by expression level, the uncentered

491 and log-transformed U133A and RPKM expression levels were used as input for

22

492   ssGSEA. Since the scores of the three signatures were not directly comparable, we

493   performed a resampling procedure to generate null distributions for each of the four

494   subtypes. First we generated a large number of virtual samples in which each gene

495   obtains its expression level by randomly selecting an expression value of the same

496   gene in the remainder of the samples. Then, the three ssGSEA scores for each

497   signature were calculated. Following this procedure we generated a large number

498   (>1,000,000) of random ssGSEA scores for each subtype, to build the null distribution

499   and to give empirical p-values for the raw ssGSEA scores of each sample. By testing on

500   multiple datasets with different sample sizes, we found the resampling generated

501   distribution could be replaced with Student-T distribution (sample size>30) or Normal

502   distribution (sample size>50) for getting very similar results. R-library with the code and

503   expression matrices used is provided as supplementary file..

504

505   ***Evaluate the simplicity of subtype activation***

506   For a single sample, we decreased rank the empirical p-values for each subtype to

507   generate order statistics as R_{N-1}, R_{N-2} ... R_1, R_0. In particular, R_0 equals to the minimum

508   empirical p-value and points to the dominant subtype, i.e., the most significantly

509   activated subtype. The accumulative distance to the dominant subtype (ADDS) was

510   defined as:

$$ADDS = \sum_{i=1}^{N-1} (R_i - R_0)$$

511   Similarly, the accumulative distance between non-dominant subtypes (ADNS) as:

$$ADNS = \sum_{j>i>0} (R_j - R_i)$$

23

512 Obviously, the ADDS and ADNS are positive and negative correlated with single

513 activation, respectively. Hence, we defined the simplicity score by combing ADDS and

514 ADNS together and corrected with a constant $\frac{(R_{N-1}-R_0)}{N-1}$ as follows:

$$Simplicity\ score = [ADDS - ADNS] \times \frac{(R_{N-1} - R_0)}{N - 1}.$$

515

516 ***Tumor purity assessment***

517 The ESTIMATE package was used to evaluate tumor purity on the basis of the

518 expression level of marker genes in stromal and immune cells (Yoshihara et al., 2013),

519 where the fraction of stromal cells and immune cells in each sample were represented

520 by stromal score and immune score respectively, and the mixed fraction of both stromal

521 and immune cells was represented by estimate scores. The ABSOLUTE package was

522 used to confirm the tumor purity on the basis of chromosome copy number and allele

523 fraction ratios on samples for which single nucleotide polymorphism array data were

524 available (Carter et al., 2012).

525

526 ***Sample collection and Neurosphere Cultures***

527 After obtaining approval from the institutional review board of The University of Texas

528 M.D. Anderson Cancer Center, glioblastoma tumor tissues were collected and named in

529 the order that they were acquired. Each tissue was enzymatically and mechanically

530 dissociated into single cells and grown in DMEM/F12 media supplemented with B27

531 (Invitrogen), EGF (20 ng/ml), and bFGF (20 ng/ml), resulting in neurosphere growth. All

532 cell lines were tested to exclude the presence of Mycoplasma infection. To minimize

533 any batch effect the downstream molecular analyses were performed on identical cell

24

534   culture batches. Total RNA from formalin fixed, paraffin embedded tumor tissues and

535   matching neurospheres was prepared using the Masterpure complete DNA and RNA

536   isolation kit (Epicenter) after proteinase K digestion per to the instructions from the

537   manufacturer. Paired-end Illumina HiSeq sequencing assays were performed resulting

538   in a medium number of 50 million 75bp paired end reads per sample. We employed the

539   PRADA pipeline to process the RNA sequencing data (Torres-Garcia et al., 2014). In

540   short, Burroughs-Wheeler alignment, Samtools, and Genome Analysis Toolkit were

541   used to map short reads to the human genome (hg19) and transcriptome (Ensembl 64)

542   and RPKM gene expression values were generated for each of the 135,994 transcripts

543   of 21,165 protein coding genes in Ensembl database.

544

545   ***Western blotting***

546   Lysates were prepared from fresh frozen sections using RPPA lysis buffer (1% Triton X-

547   100 50mM HEPES pH 7.4, 150mM NaCl, 1.5mM MgCl2, 1mM EGTA, 100mM NaF,

548   10mM Na pyrophosphate, 1mM Na3VO4, 10% glycerol, plus protease and phosphatase

549   inhibitors cocktails from Roche Applied Science #05056489001 and 04906837001), with

550   sonication and clearing by centrifugation at 10,000g. Protein concentration was

551   measured using the BCA kit (Thermo Scientific - Pierce #23225). SDS-PAGE and

552   western blotting was performed using Midi gel system (Life Technologies - #WR0100)

553   and NuPage-Novex 4-12% Bis-Tris Midi (20-well) Protein Gels (Life Technologies -

554   #WG1402) using the following antibodies: ITGAM (CD11B) (Sigma Aldrich –

555   #HPA002274), IBA1 (AIF1) (Sigma Aldrich – #HPA049234), GFAP (Cell Signalling –

556 #3670), YKL40 (CHI3L1) YKL40 (CHI3L1, Santa Cruz Biotechnology - #sc-30465) a-

557 actinin (Sigma Aldrich A5044) and Tubulin (Sigma Aldrich T9026).

558

559 ***Immunohistochemistry***

560 Formalin-fixed, paraffin-embedded tissue sections (4 μm thick) were collected on

561 Superfrost plus slides. Briefly, tissue sections were deparaffinized with xylene and

562 ethanol and re-hydrated with 95, 70 and 50% ethanol. Sections were antigen unmasked

563 using citrate buffer (Vector Labs #H-3300) and heating. Peroxidase block was

564 conducted with 3% H2O2 and blocking was with 5% goat serum (Vector Labs #S-1000).

565 Primary rabbit polyconal antibody against IBA1 (AIF1)(WAKO #016-20001) at 1:400

566 was used overnight. Secondary antibody was done using with the Rabbit-on-Rodent

567 HRP-Polymer (Biocare #RMR622L) for 1 hr at room temperature. The slides were

568 developed with Nova-red (Vector Labs #SK-4800) and counterstained with

569 haematoxylin, mounted and scanned with Pannoramic 250 slide scanner (Caliper Life

570 Sciences). Unbiased quantification of microglial (IBA1+) percentage in primary and

571 recurrent GBMs was performed using the Caliper Vectra image system and InForm

572 analysis software. Thirty scan fields were automatically selected on from entire tumor

573 section. Nineteen scan fields were select from the primary tumor of patient #2 due to the

574 small size of tumor section. Percentages of the median and high levels (2+, 3+) of IBA1

575 were used for the comparison.

576

Acknowledgments

594

595 **References**

596 Aran, D., Sirota, M., and Butte, A. J. (2015). Systematic pan-cancer analysis of tumour purity. Nat
597 Commun *6*, 8971.
598 Bao, S., Wu, Q., McLendon, R. E., Hao, Y., Shi, Q., Hjelmeland, A. B., Dewhirst, M. W., Bigner, D. D., and
599 Rich, J. N. (2006). Glioma stem cells promote radioresistance by preferential activation of the DNA
600 damage response. Nature *444*, 756-760.
601 Barbie, D. A., Tamayo, P., Boehm, J. S., Kim, S. Y., Moody, S. E., Dunn, I. F., Schinzel, A. C., Sandy, P.,
602 Meylan, E., Scholl, C., *et al.* (2009). Systematic RNA interference reveals that oncogenic KRAS-driven
603 cancers require TBK1. Nature *462*, 108-112.
604 Baysan, M., Bozdag, S., Cam, M. C., Kotliarova, S., Ahn, S., Walling, J., Killian, J. K., Stevenson, H., Meltzer,
605 P., and Fine, H. A. (2012). G-cimp status prediction of glioblastoma samples using mRNA expression data.
606 PloS one *7*, e47839.
607 Bengtsson, H., Ray, A., Spellman, P., and Speed, T. P. (2009). A single-sample method for normalizing and
608 combining full-resolution copy numbers from multiple platforms, labs and analysis methods.
609 Bioinformatics *25*, 861-867.
610 Bhat, K. P., Balasubramaniyan, V., Vaillant, B., Ezhilarasan, R., Hummelink, K., Hollingsworth, F., Wani, K.,
611 Heathcock, L., James, J. D., Goodman, L. D., *et al.* (2013). Mesenchymal differentiation mediated by NF-
612 kappaB promotes radiation resistance in glioblastoma. Cancer cell *24*, 331-346.
613 Blank, C. U., Haanen, J. B., Ribas, A., and Schumacher, T. N. (2016). CANCER IMMUNOLOGY. The "cancer
614 immunogram". Science *352*, 658-660.
615 Brennan, C. W., Verhaak, R. G., McKenna, A., Campos, B., Noushmehr, H., Salama, S. R., Zheng, S.,
616 Chakravarty, D., Sanborn, J. Z., Berman, S. H., *et al.* (2013). The somatic genomic landscape of
617 glioblastoma. Cell *155*, 462-477.
618 Cancer Genome Atlas Research, N. (2008). Comprehensive genomic characterization defines human
619 glioblastoma genes and core pathways. Nature *455*, 1061-1068.
620 Cancer Genome Atlas Research, N., Brat, D. J., Verhaak, R. G., Aldape, K. D., Yung, W. K., Salama, S. R.,
621 Cooper, L. A., Rheinbay, E., Miller, C. R., Vitucci, M., *et al.* (2015). Comprehensive, Integrative Genomic
622 Analysis of Diffuse Lower-Grade Gliomas. N Engl J Med *372*, 2481-2498.
623 Carter, S. L., Cibulskis, K., Helman, E., McKenna, A., Shen, H., Zack, T., Laird, P. W., Onofrio, R. C.,
624 Winckler, W., Weir, B. A., *et al.* (2012). Absolute quantification of somatic DNA alterations in human
625 cancer. Nat Biotechnol *30*, 413-421.
626 Ceccarelli, M., Barthel, F. P., Malta, T. M., Sabedot, T. S., Salama, S. R., Murray, B. A., Morozova, O.,
627 Newton, Y., Radenbaugh, A., Pagnotta, S. M., *et al.* (2016). Molecular Profiling Reveals Biologically
628 Discrete Subsets and Pathways of Progression in Diffuse Glioma. Cell *164*, 550-563.
629 Dai, M., Wang, P., Boyd, A. D., Kostov, G., Athey, B., Jones, E. G., Bunney, W. E., Myers, R. M., Speed, T.
630 P., Akil, H., *et al.* (2005). Evolving gene/transcript definitions significantly alter the interpretation of
631 GeneChip data. Nucleic Acids Res *33*, e175.
632 Deng, L., Liang, H., Burnette, B., Beckett, M., Darga, T., Weichselbaum, R. R., and Fu, Y. X. (2014).
633 Irradiation and anti-PD-L1 treatment synergistically promote antitumor immunity in mice. J Clin Invest
634 *124*, 687-695.
635 Doucette, T., Rao, G., Rao, A., Shen, L., Aldape, K., Wei, J., Dziurzynski, K., Gilbert, M., and Heimberger, A.
636 B. (2013). Immune heterogeneity of glioblastoma subtypes: extrapolation from the cancer genome atlas.
637 Cancer Immunol Res *1*, 112-122.
638 Dunn, G. P., Rinne, M. L., Wykosky, J., Genovese, G., Quayle, S. N., Dunn, I. F., Agarwalla, P. K., Chheda,
639 M. G., Campos, B., Wang, A., *et al.* (2012). Emerging insights into the molecular and cellular basis of
640 glioblastoma. Genes Dev *26*, 756-784.
641 Engler, J. R., Robinson, A. E., Smirnov, I., Hodgson, J. G., Berger, M. S., Gupta, N., James, C. D., Molinaro,
642 A., and Phillips, J. J. (2012). Increased microglia/macrophage gene expression in a subset of adult and
643 pediatric astrocytomas. PLoS One *7*, e43339.
644 Gabrusiewicz, K., Rodriguez, B., Wei, J., Hashimoto, Y., Healy, L. M., Maiti, S. N., Thomas, G., Zhou, S.,
645 Wang, Q., Elakkad, A., *et al.* (2016). Glioblastoma-infiltrated innate immune cells resemble M0
646 macrophage phenotype. JCI insight *1*.

647   Galli, R., Binda, E., Orfanelli, U., Cipelletti, B., Gritti, A., De Vitis, S., Fiocco, R., Foroni, C., Dimeco, F., and
648   Vescovi, A. (2004). Isolation and characterization of tumorigenic, stem-like neural precursors from
649   human glioblastoma. Cancer Res *64*, 7011-7021.
650   Gill, B. J., Pisapia, D. J., Malone, H. R., Goldstein, H., Lei, L., Sonabend, A., Yun, J., Samanamud, J., Sims, J.
651   S., Banu, M., *et al.* (2014). MRI-localized biopsies reveal subtype-specific differences in molecular and
652   cellular composition at the margins of glioblastoma. Proc Natl Acad Sci U S A *111*, 12550-12555.
653   Hambardzumyan, D., Gutmann, D. H., and Kettenmann, H. (2015). The role of microglia and
654   macrophages in glioma maintenance and progression. Nature neuroscience *19*, 20-27.
655   Hunter, C., Smith, R., Cahill, D. P., Stephens, P., Stevens, C., Teague, J., Greenman, C., Edkins, S., Bignell,
656   G., Davies, H., *et al.* (2006). A hypermutation phenotype and somatic MSH6 mutations in recurrent
657   human malignant gliomas after alkylator chemotherapy. Cancer Res *66*, 3987-3991.
658   Huse, J. T., Phillips, H. S., and Brennan, C. W. (2011). Molecular subclassification of diffuse gliomas:
659   seeing order in the chaos. Glia *59*, 1190-1199.
660   Isella, C., Terrasi, A., Bellomo, S. E., Petti, C., Galatola, G., Muratore, A., Mellano, A., Senetta, R., Cassenti,
661   A., Sonetto, C., *et al.* (2015). Stromal contribution to the colorectal cancer transcriptome. Nat Genet *47*,
662   312-319.
663   Joo, K. M., Kim, J., Jin, J., Kim, M., Seol, H. J., Muradov, J., Yang, H., Choi, Y. L., Park, W. Y., Kong, D. S., *et*
664   *al.* (2013). Patient-specific orthotopic glioblastoma xenograft models recapitulate the histopathology
665   and biology of human glioblastomas in situ. Cell Rep *3*, 260-273.
666   Kim, H., and Verhaak, R. G. (2015). Transcriptional mimicry by tumor-associated stroma. Nat Genet *47*,
667   307-309.
668   Kim, H., Zheng, S., Amini, S. S., Virk, S. M., Mikkelsen, T., Brat, D. J., Grimsby, J., Sougnez, C., Muller, F.,
669   Hu, J., *et al.* (2015). Whole-genome and multisector exome sequencing of primary and post-treatment
670   glioblastoma reveals patterns of tumor evolution. Genome Res *25*, 316-327.
671   Kreutzberg, G. W. (1996). Microglia: a sensor for pathological events in the CNS. Trends Neurosci *19*,
672   312-318.
673   Kwon, S. M., Kang, S. H., Park, C. K., Jung, S., Park, E. S., Lee, J. S., Kim, S. H., and Woo, H. G. (2015).
674   Recurrent Glioblastomas Reveal Molecular Subtypes Associated with Mechanistic Implications of Drug-
675   Resistance. PLoS One *10*, e0140528.
676   Le, L. Q., Shipman, T., Burns, D. K., and Parada, L. F. (2009). Cell of origin and microenvironment
677   contribution for NF1-associated dermal neurofibromas. Cell Stem Cell *4*, 453-463.
678   Martinez, E., Yoshihara, K., Kim, H., Mills, G. M., Trevino, V., and Verhaak, R. G. (2015). Comparison of
679   gene expression patterns across 12 tumor types identifies a cancer supercluster characterized by TP53
680   mutations and cell cycle defects. Oncogene *34*, 2732-2740.
681   Mazor, T., Pankov, A., Johnson, B. E., Hong, C., Hamilton, E. G., Bell, R. J., Smirnov, I. V., Reis, G. F.,
682   Phillips, J. J., Barnes, M. J., *et al.* (2015). DNA Methylation and Somatic Mutations Converge on the Cell
683   Cycle and Define Similar Evolutionary Histories in Brain Tumors. Cancer Cell *28*, 307-317.
684   Meng, Y., Beckett, M. A., Liang, H., Mauceri, H. J., van Rooijen, N., Cohen, K. S., and Weichselbaum, R. R.
685   (2010). Blockade of tumor necrosis factor alpha signaling in tumor-associated macrophages as a
686   radiosensitizing strategy. Cancer research *70*, 1534-1543.
687   Newman, A. M., Liu, C. L., Green, M. R., Gentles, A. J., Feng, W., Xu, Y., Hoang, C. D., Diehn, M., and
688   Alizadeh, A. A. (2015). Robust enumeration of cell subsets from tissue expression profiles. Nat Methods
689   *12*, 453-457.
690   Noushmehr, H., Weisenberger, D. J., Diefes, K., Phillips, H. S., Pujara, K., Berman, B. P., Pan, F., Pelloski, C.
691   E., Sulman, E. P., Bhat, K. P., *et al.* (2010). Identification of a CpG island methylator phenotype that
692   defines a distinct subgroup of glioma. Cancer Cell *17*, 510-522.
693   Olar, A., and Aldape, K. D. (2014). Using the molecular classification of glioblastoma to inform
694   personalized treatment. The Journal of pathology *232*, 165-177.
695   Ozawa, T., Riester, M., Cheng, Y., Huse, J. T., Squatrito, M., Helmy, K., Charles, N., Michor, F., and
696   Holland, E. C. (2014). Most human non-GCIMP glioblastoma subtypes evolve from a common proneural-
697   like precursor glioma. Cancer Cell *26*, 288-300.
698   Palucka, K., and Banchereau, J. (2012). Cancer immunotherapy via dendritic cells. Nature reviews Cancer
699   *12*, 265-277.

700 Patel, A. P., Tirosh, I., Trombetta, J. J., Shalek, A. K., Gillespie, S. M., Wakimoto, H., Cahill, D. P., Nahed, B.
701 V., Curry, W. T., Martuza, R. L., *et al.* (2014). Single-cell RNA-seq highlights intratumoral heterogeneity in
702 primary glioblastoma. Science *344*, 1396-1401.
703 Phillips, H. S., Kharbanda, S., Chen, R., Forrest, W. F., Soriano, R. H., Wu, T. D., Misra, A., Nigro, J. M.,
704 Colman, H., Soroceanu, L., *et al.* (2006). Molecular subclasses of high-grade glioma predict prognosis,
705 delineate a pattern of disease progression, and resemble stages in neurogenesis. Cancer Cell *9*, 157-173.
706 Prins, R. M., Soto, H., Konkankit, V., Odesa, S. K., Eskin, A., Yong, W. H., Nelson, S. F., and Liau, L. M.
707 (2011). Gene expression profile correlates with T-cell infiltration and relative survival in glioblastoma
708 patients vaccinated with dendritic cell immunotherapy. Clin Cancer Res *17*, 1603-1615.
709 Pyonteck, S. M., Akkari, L., Schuhmacher, A. J., Bowman, R. L., Sevenich, L., Quail, D. F., Olson, O. C.,
710 Quick, M. L., Huse, J. T., Teijeiro, V., *et al.* (2013). CSF-1R inhibition alters macrophage polarization and
711 blocks glioma progression. Nat Med *19*, 1264-1272.
712 Ries, C. H., Cannarile, M. A., Hoves, S., Benz, J., Wartha, K., Runza, V., Rey-Giraud, F., Pradel, L. P.,
713 Feuerhake, F., Klaman, I., *et al.* (2014). Targeting tumor-associated macrophages with anti-CSF-1R
714 antibody reveals a strategy for cancer therapy. Cancer Cell *25*, 846-859.
715 Ruffell, B., and Coussens, L. M. (2015). Macrophages and therapeutic resistance in cancer. Cancer cell *27*,
716 462-472.
717 Sandberg, R., and Larsson, O. (2007). Improved precision and accuracy for microarrays using updated
718 probe set definitions. BMC Bioinformatics *8*, 48.
719 Schumacher, T. N., and Schreiber, R. D. (2015). Neoantigens in cancer immunotherapy. Science *348*, 69-
720 74.
721 Sturm, D., Bender, S., Jones, D. T., Lichter, P., Grill, J., Becher, O., Hawkins, C., Majewski, J., Jones, C.,
722 Costello, J. F., *et al.* (2014). Paediatric and adult glioblastoma: multiform (epi)genomic culprits emerge.
723 Nat Rev Cancer *14*, 92-107.
724 Sturm, D., Witt, H., Hovestadt, V., Khuong-Quang, D. A., Jones, D. T., Konermann, C., Pfaff, E., Tonjes, M.,
725 Sill, M., Bender, S., *et al.* (2012). Hotspot mutations in H3F3A and IDH1 define distinct epigenetic and
726 biological subgroups of glioblastoma. Cancer Cell *22*, 425-437.
727 Torres-Garcia, W., Zheng, S., Sivachenko, A., Vegesna, R., Wang, Q., Yao, R., Berger, M. F., Weinstein, J.
728 N., Getz, G., and Verhaak, R. G. (2014). PRADA: pipeline for RNA sequencing data analysis. Bioinformatics
729 *30*, 2224-2226.
730 Verhaak, C. M., Lintsen, A. M., Evers, A. W., and Braat, D. D. (2010a). Who is at risk of emotional
731 problems and how do you know? Screening of women going for IVF treatment. Hum Reprod *25*, 1234-
732 1240.
733 Verhaak, R. G., Hoadley, K. A., Purdom, E., Wang, V., Qi, Y., Wilkerson, M. D., Miller, C. R., Ding, L., Golub,
734 T., Mesirov, J. P., *et al.* (2010b). Integrated genomic analysis identifies clinically relevant subtypes of
735 glioblastoma characterized by abnormalities in PDGFRA, IDH1, EGFR, and NF1. Cancer Cell *17*, 98-110.
736 Verhaak, R. G., Tamayo, P., Yang, J. Y., Hubbard, D., Zhang, H., Creighton, C. J., Fereday, S., Lawrence, M.,
737 Carter, S. L., Mermel, C. H., *et al.* (2013). Prognostically relevant gene signatures of high-grade serous
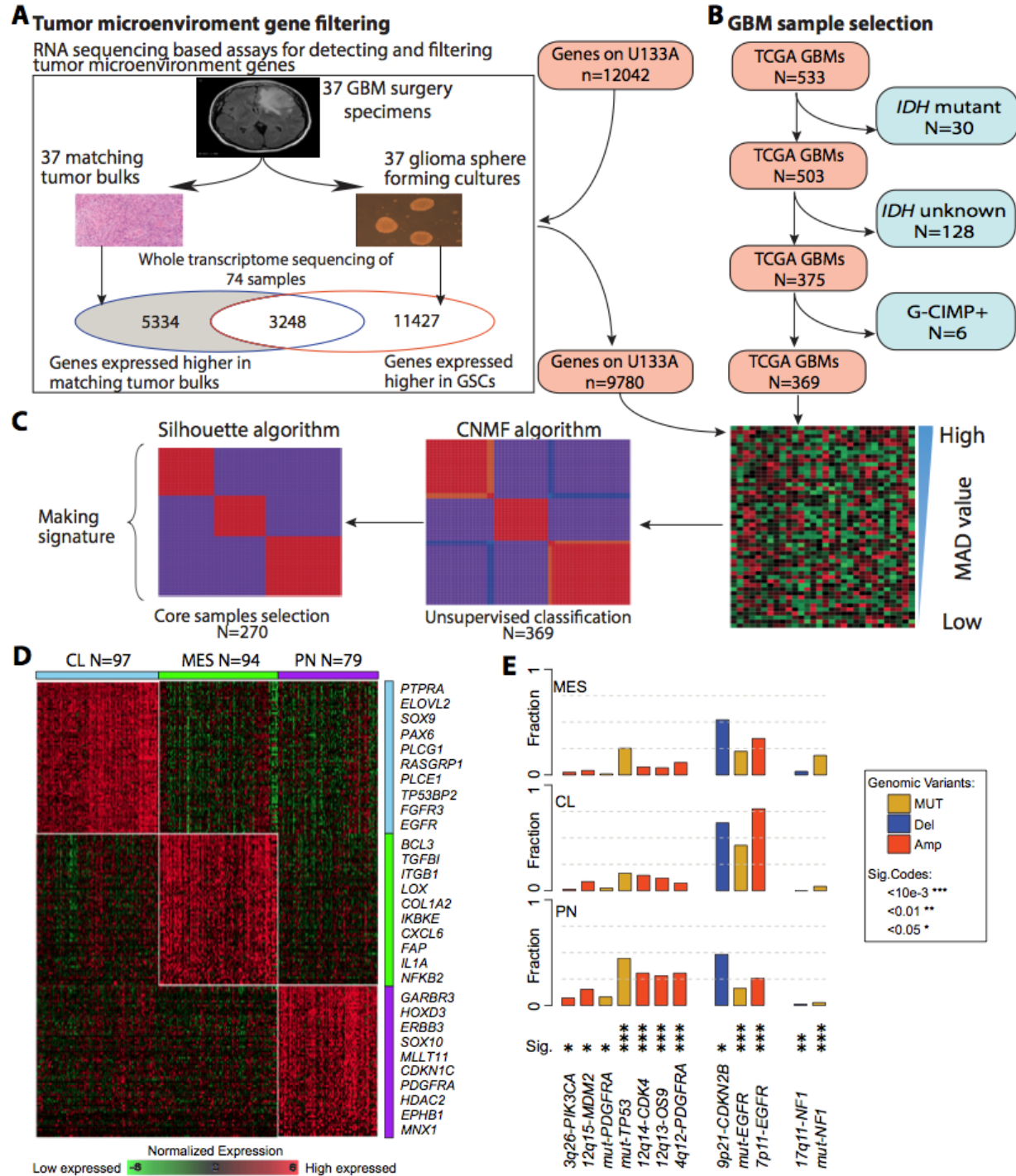738 ovarian carcinoma. J Clin Invest *123*, 517-525.
739 Yan, J., Kong, L. Y., Hu, J., Gabrusiewicz, K., Dibra, D., Xia, X., Heimberger, A. B., and Li, S. (2015). FGL2 as
740 a Multimodality Regulator of Tumor-Mediated Immune Suppression and Therapeutic Target in Gliomas.
741 J Natl Cancer Inst *107*.
742 Ye, X. Z., Xu, S. L., Xin, Y. H., Yu, S. C., Ping, Y. F., Chen, L., Xiao, H. L., Wang, B., Yi, L., Wang, Q. L., *et al.*
743 (2012). Tumor-associated microglia/macrophages enhance the invasion of glioma stem-like cells via TGF-
744 beta1 signaling pathway. J Immunol *189*, 444-453.
745 Yoshihara, K., Shahmoradgoli, M., Martinez, E., Vegesna, R., Kim, H., Torres-Garcia, W., Trevino, V., Shen,
746 H., Laird, P. W., Levine, D. A., *et al.* (2013). Inferring tumour purity and stromal and immune cell
747 admixture from expression data. Nat Commun *4*, 2612.
748 Zeng, J., See, A. P., Phallen, J., Jackson, C. M., Belcaid, Z., Ruzevick, J., Durham, N., Meyer, C., Harris, T. J.,
749 Albesiano, E., *et al.* (2013). Anti-PD-1 blockade and stereotactic radiation produce long-term survival in
750 mice with intracranial gliomas. Int J Radiat Oncol Biol Phys *86*, 343-349.
751 Zheng, S., Chheda, M. G., and Verhaak, R. G. (2012). Studying a complex tumor: potential and pitfalls.
752 Cancer J *18*, 107-114.

Figure 1. Molecular classification of IDHwt GBMs. (A) Filtering tumor associated microenvironment genes. (**B**) Discarding IDH mutation related GBMs. (**C**) Overview of NMF clustering. (**D**) Heatmap of 70-gene signatures by gene expression subtype were developed based on 270 GBMs. Top ten genes are shown for each subtype. (**E**) Frequency of subtype related somatic genomic alterations. Chi-square test was used to calculate the distribution difference among three subtypes per genomic variant.
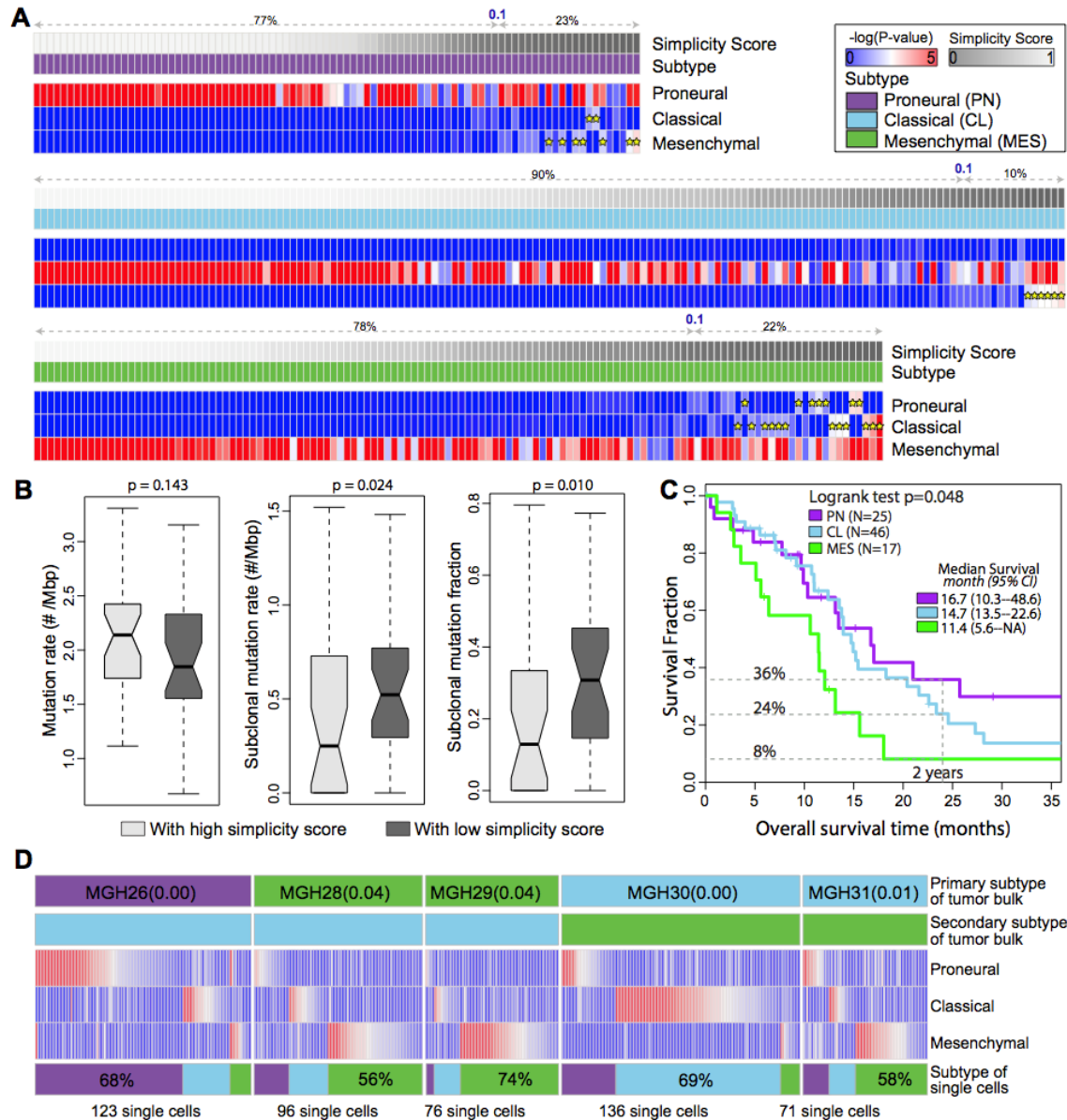
Figure 2. Multi activation of transcriptional subtypes associated with intratumoral heterogeneity. (**A**) The expression profiles of 369 IDHwt GBMs were analyzed using Affymetrix U133A. The empirical -log(empirical P-value) of raw ssGSEA enrichment scores at each signature are shown as heatmaps, with dark blue representing no activation and bright red as highly activated. Yellow star indicates the secondary activated subtype (empirical p-value<0.05). For each panel, the first row shows simplicity score, and the second row indicates transcriptional subtype. (**B**) Comparison of mutation rate, subclonal mutation rate and subclonal mutation fraction between IDHwt GBMs with high and low simplicity scores. P-values were calculated using Wilcoxon rank test and shown at the top of each panel. (**C**) Kaplan-Meier survival curve by subtype. (**D**) Transcriptome classification of five bulk tumor samples and 502 single GBM cells derived from them. The top two row of each panel show the dominant and secondary subtype of the GBM tumor bulk. The heatmap of each panel shows the empirical -log(P-value) of the ssGSEA scores of the derived single GBM cells on each of the three subtype signatures. The bottom row shows the subtype distribution of derived single GBM cells within the same GBM tumor of origin.
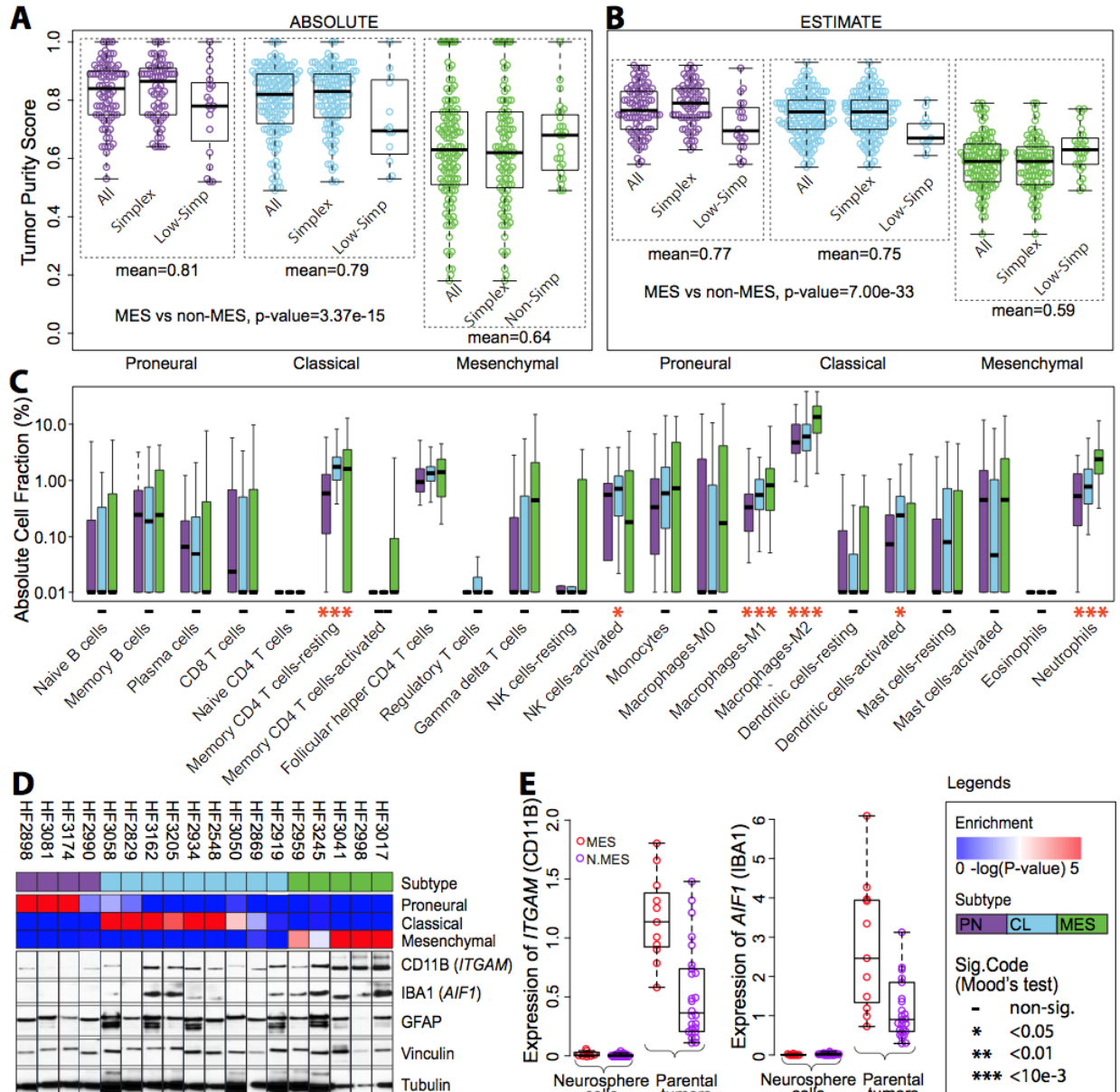
**Figure 3. Transcriptional subtypes differentially activate the immune microenvironment.** (**A, B**) Tumor purity of 364 respectively 369 TCGA IDHwt GBM samples was determined by ABSOLUTE and ESTIMATE. The difference in tumor purity between subtypes was evaluated using a two-sample heteroscedastic t-test. (**C**) Comparison of immune cell fractions among subtypes. Immune cell fractions were estimated using CIBERSORT and corrected using ABSOLUTE purity scores per sample. The distribution of immune cell fractions of 69 PN, 137 CL and 96 MES IDHwt GBMs with simplicity score>0.1 were shown by purple, skyblue and green boxplots, respectively. Median value difference of cell fraction among subtypes was evaluated using Mood's test. (**D**) The upper panel shows ssGSEA enrichment scores and associated expression subtype classifications. Bottom panels display protein expression of the microglial markers integrin alpha M (ITGAM) and allograft inflammatory factor 1 (IBA1), astrocyte marker glial fibrillary acidic protein (GFAP) and the loading control tubulin. (**E**) Comparison of *ITGAM* and *IBA1* gene expression levels between GBM and derived neurosphere models.
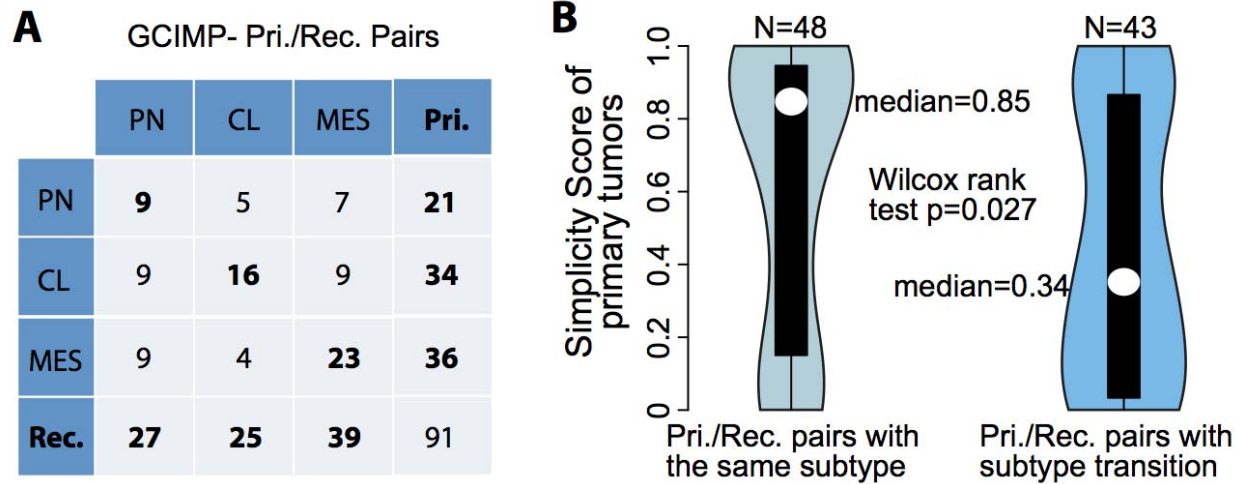
Figure 4. Comparison between transcriptional subtype of primary and paired recurrent tumors. (**A**) Rows and columns of the cross table represents subtype distribution frequency of primary and paired recurrent tumors, respectively. (**B**) Violin plots show the distribution of simplicity scores of pairs with (left) and without (right) subtype transition.
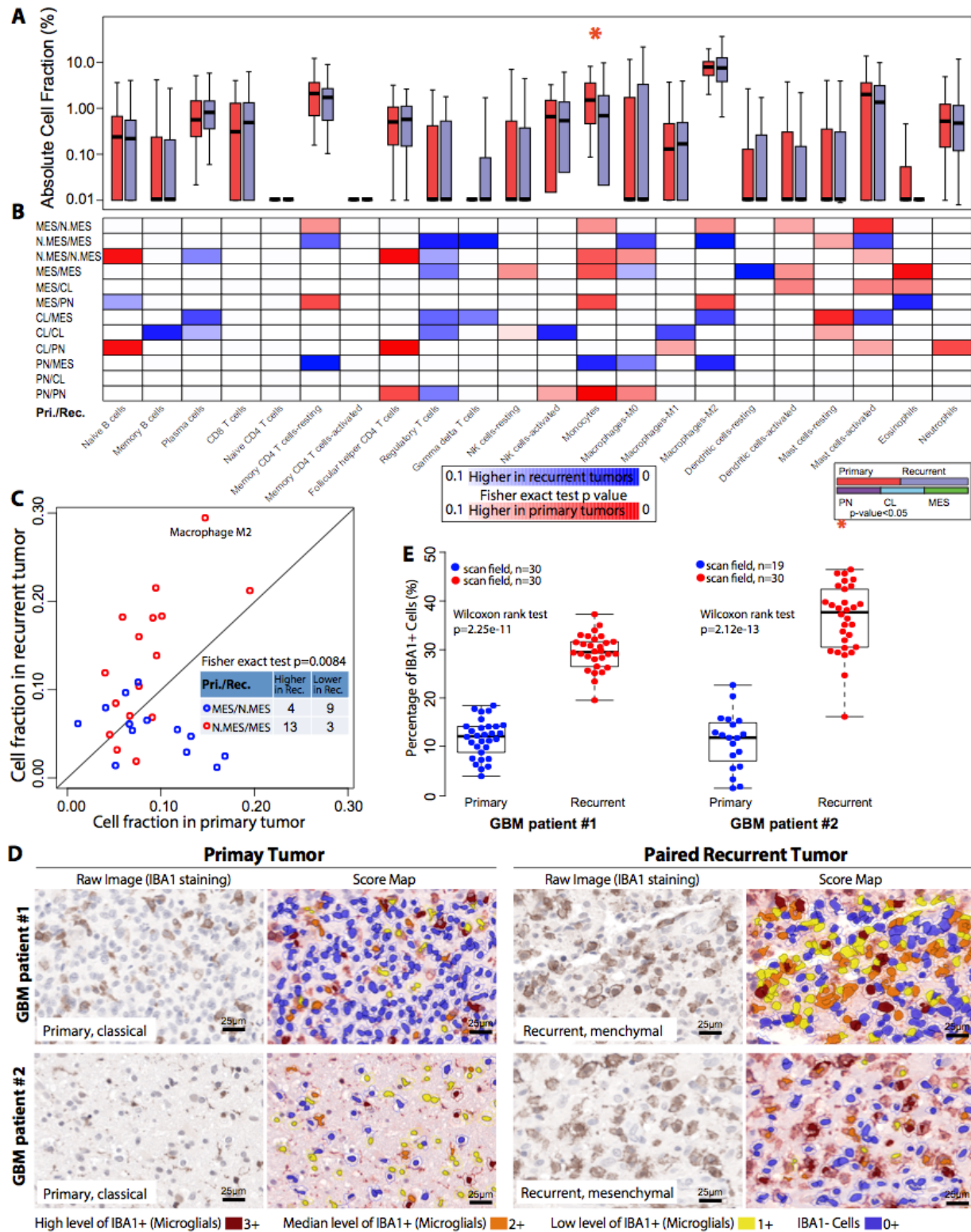
Figure 5. Microenvironment transition between 91 primary and paired recurrent IDH wild type GBM. (**A**) Red and blue boxplots represent the immune cell fraction distribution of each immune cell type. Immune cell fraction was calculated using CIBERSORT and adjusted using ESTIMATE purity scores. Difference between cell fraction of primary and paired recurrent tumors was calculated using Wilcoxon rank test. (**B**) The blue-to-red heatmap represents

35

805   immune cell fraction changes upon tumor recurrence per subtype transitions which were list on
806   the left of the heatmap. Fisher exact test was used to evaluate the distribution difference
807   between patients with higher/lower immune cell fractions at tumor recurrence per subtype
808   transition. (**C**) Each dot represents a pair of primary and recurrent GBM with axes indicating M2
809   macrophage cell fraction. (**D**) Representative images of IBA1 immunohistochemical staining and
810   corresponding score map obtained by InForm image analysis in two matched pairs of primary
811   and recurrent GBM. Scale bar, 25 µm. **(E)** Unbiased quantification of IBA1+ percentage in
812   primary and recurrent GBMs.
813
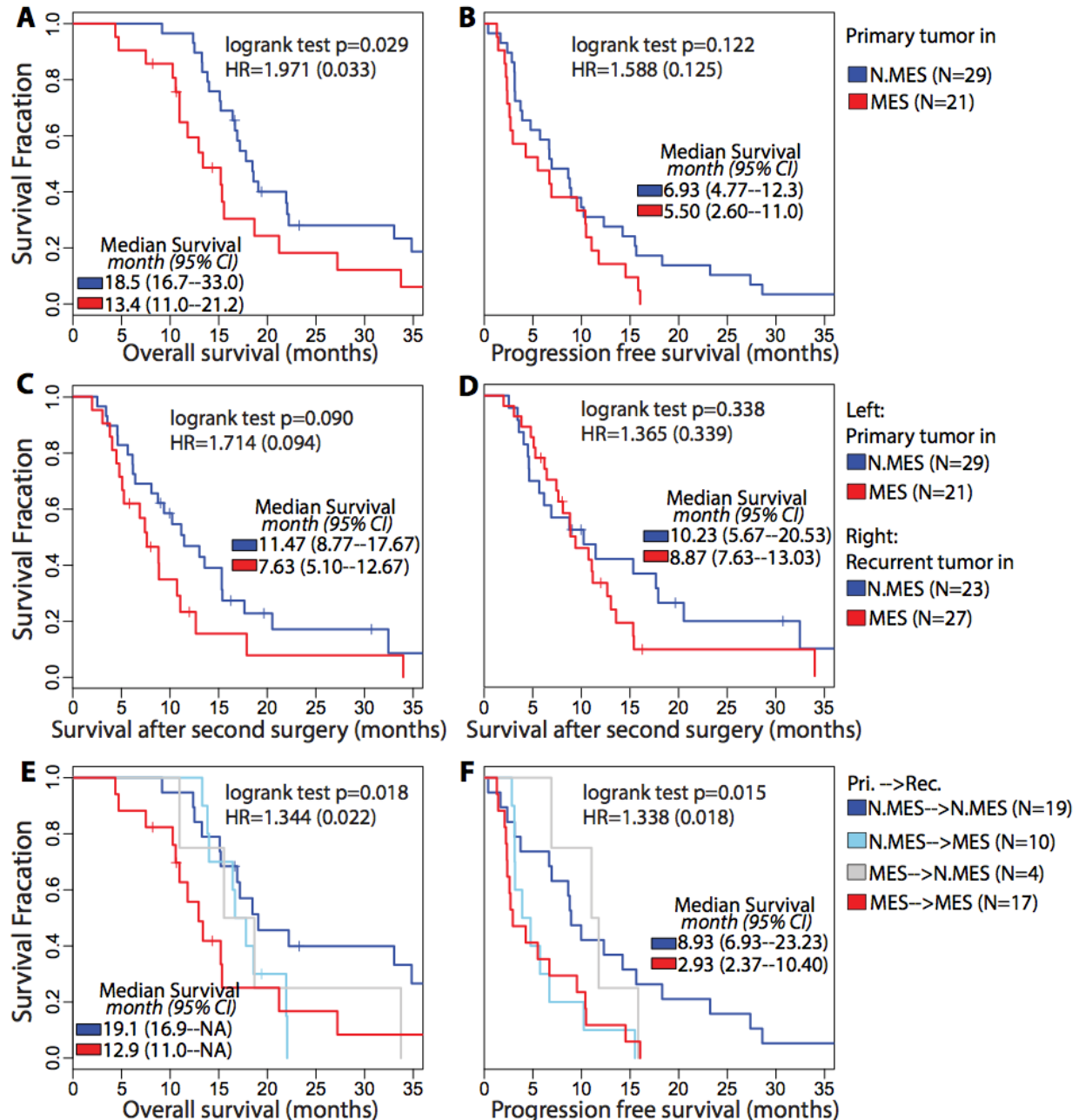
Figure 6. Survival analysis of paired IDH wild type GBM. (**A, B**) OS and PFS analyses between samples with different primary subtype. (**C**) Difference of survival time after secondary surgery between patients with non-MES and MES in primary tumors. (**D**) Survival analysis of time after secondary surgery between patients with non-MES and MES in recurrent tumors. (E, F) OS and PFS analyses between samples with difference recurrent subtype.
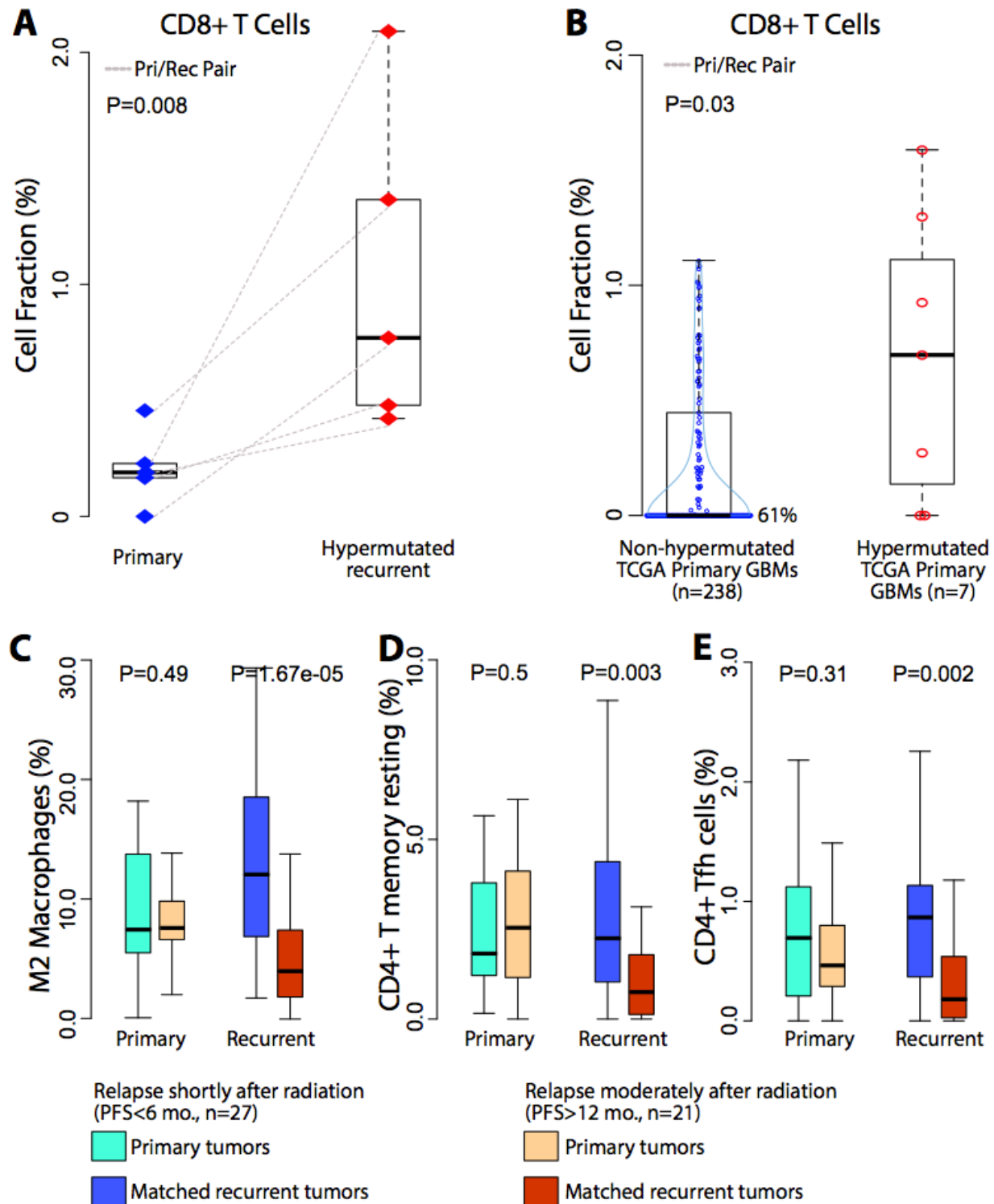
Figure 7. Immune cell frequency comparison. (**A**). Blue and red diamond indicate individual primary and recurrent tumors. Dash line connects paired primary and recurrent tumors. (**B**). Blue and red cycle indicate non-hypermutated and hypermutated primary samples. (**C-E**). Sky blue/dark blue and orange/red boxplots indicate short- and long- term relapsed tumors,

826   respectively. Wilcoxon rank tests were used to examine the significance of the differences
827   between groups.
828

Supplementary Information
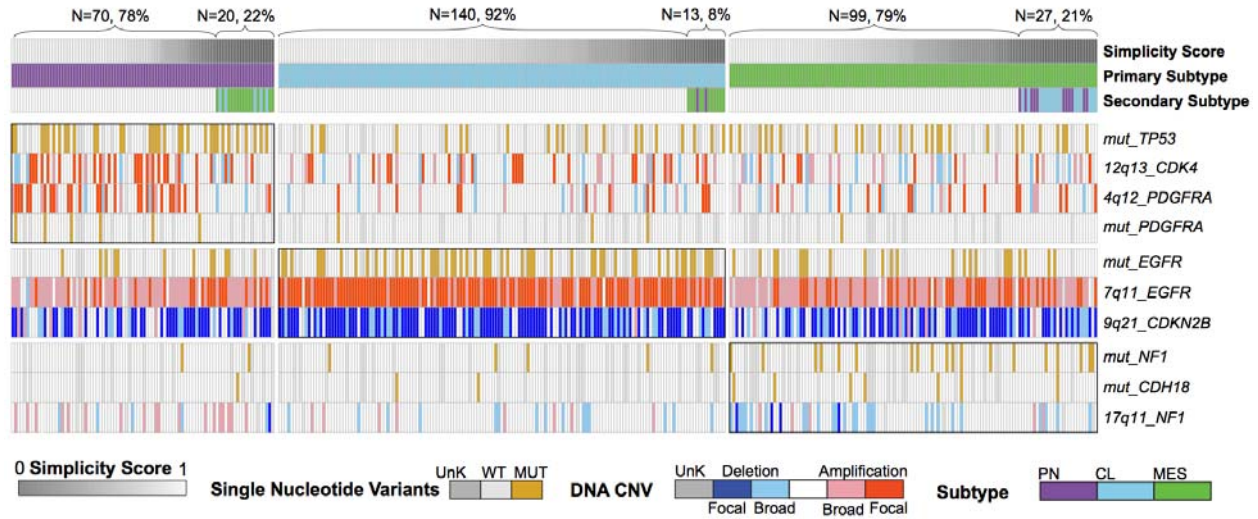
829

Supplementary Figures and Legends

830

831
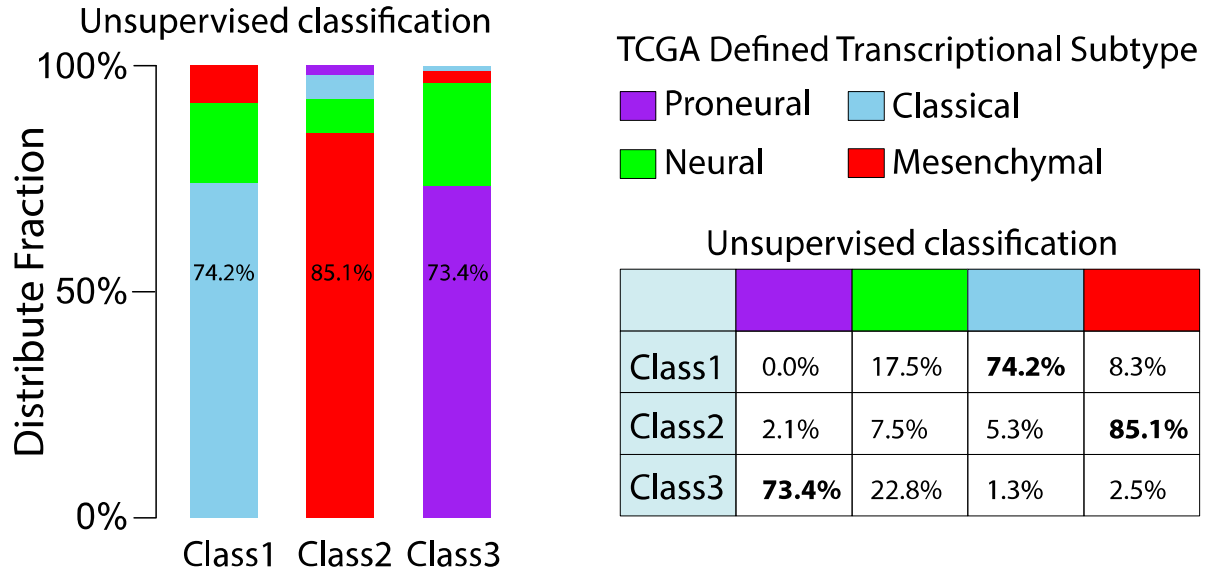
Figure S1. Comparison between GCIMP- GBM specific classification and TCGA defined GBM subtypes. 270 samples were identified as core samples with positive silhouette width core samples. 97, 94 and 79 samples were unsupervised classified class1, class2 and class3, respectively. The previous four transcriptional subtypes of these 270 samples were determined by TCGA Research Network (Brennan et al., 2013).
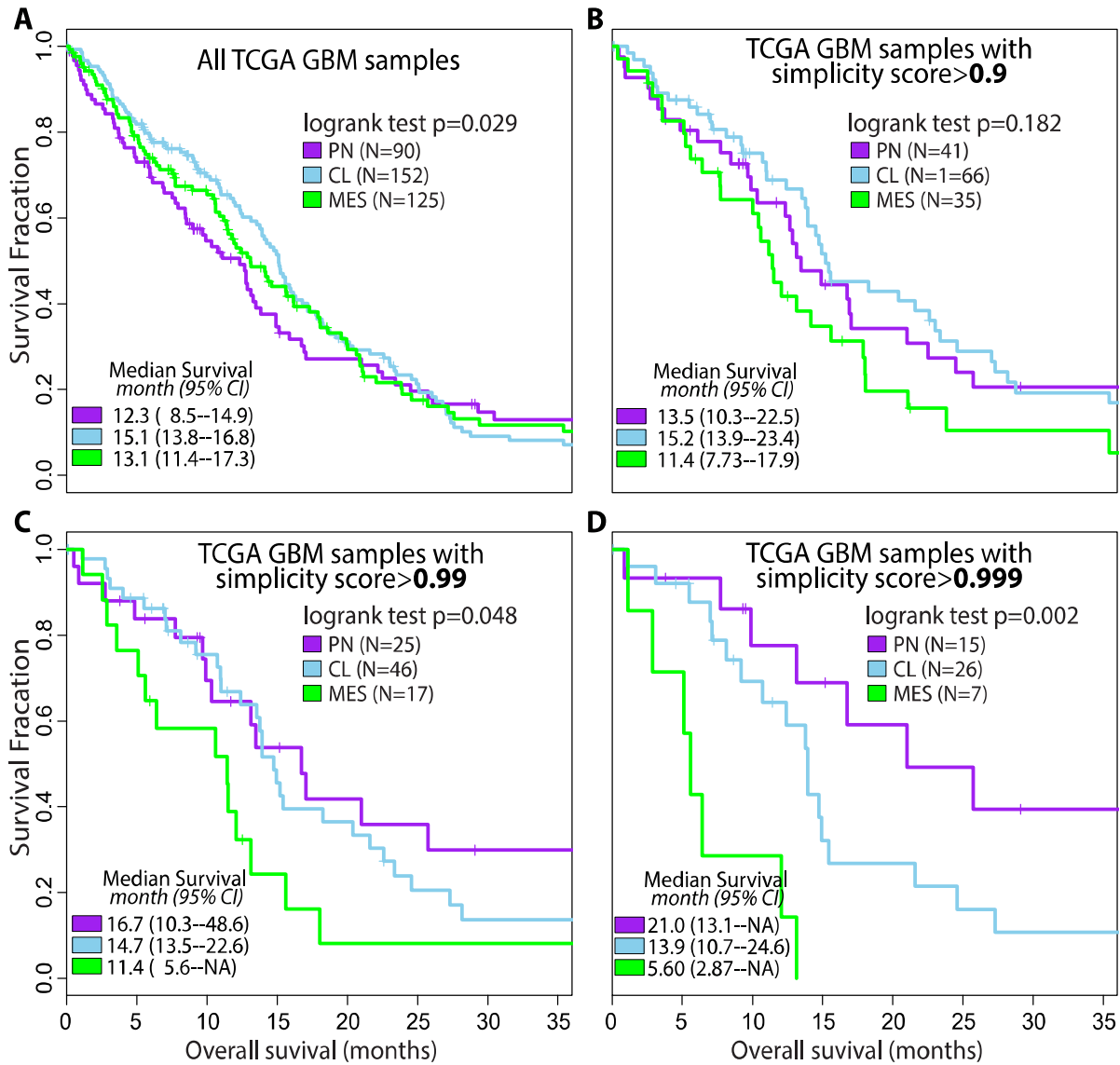
832
833
834
835
836
837

838

839
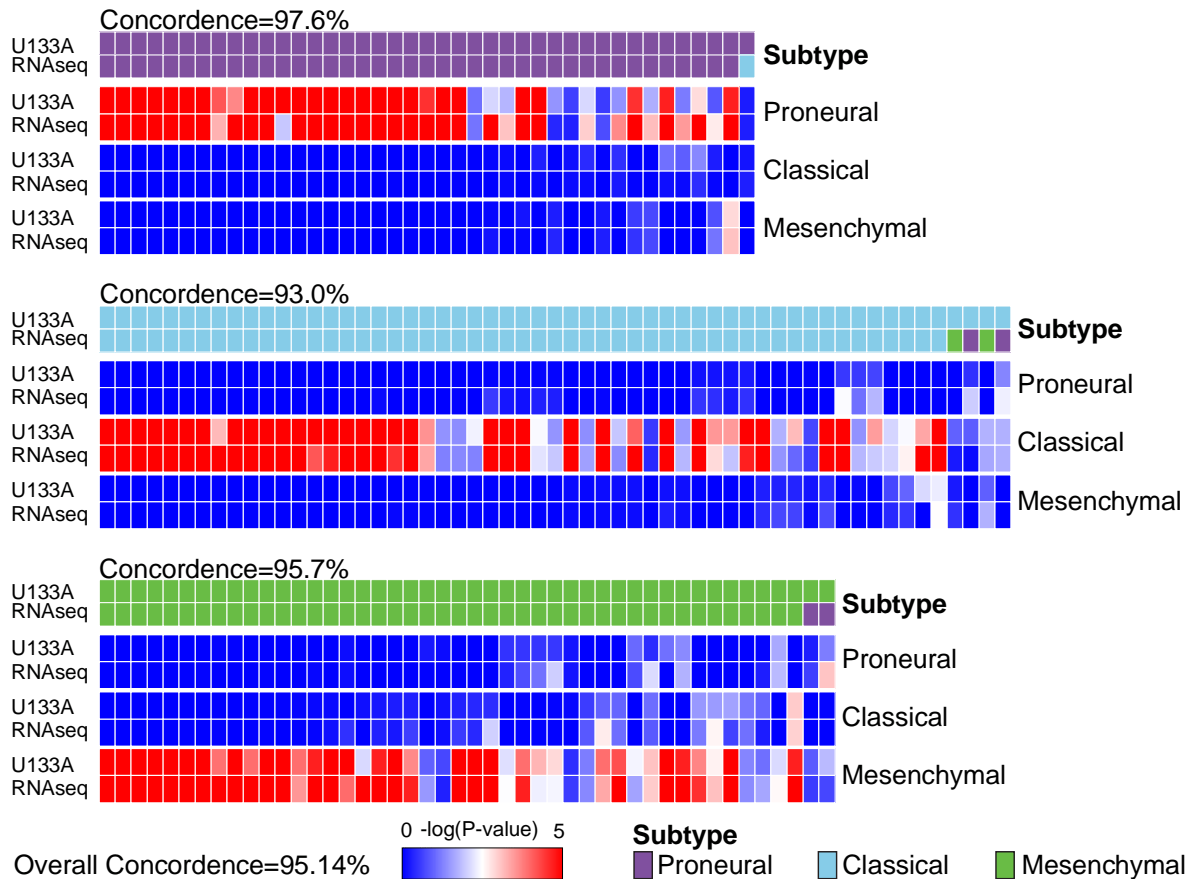
Figure S2. Concordance of transcriptional classification of GBMs crosses multiple platforms. Through TCGA, the expression profiles of 144 GBM were analyzed using both Affymetrix U133A gene expression arrays and RNA sequencing. The empirical -log(P-value) of raw ssGSEA enrichment scores at each signature are shown as heatmaps, with dark blue representing no activation and bright red as highly activated. For each panel, the first row shows U133A based classification, and the second row indicates RNA-seq subtype classification.

846

847

Figure S3. Genomic alteration patterns for each subtype. Ten prominent GBM somatic events were manually selected. Simplicity score and primary subtype were shown by the first two rows. For samples with simplicity score less than 0.1, the secondary subtype was also shown by the third row.

852

853

Figure S4. Patient survival differences between transcriptional subtypes. Samples were filtered using increased simplicity score as threshold from panel A to D.
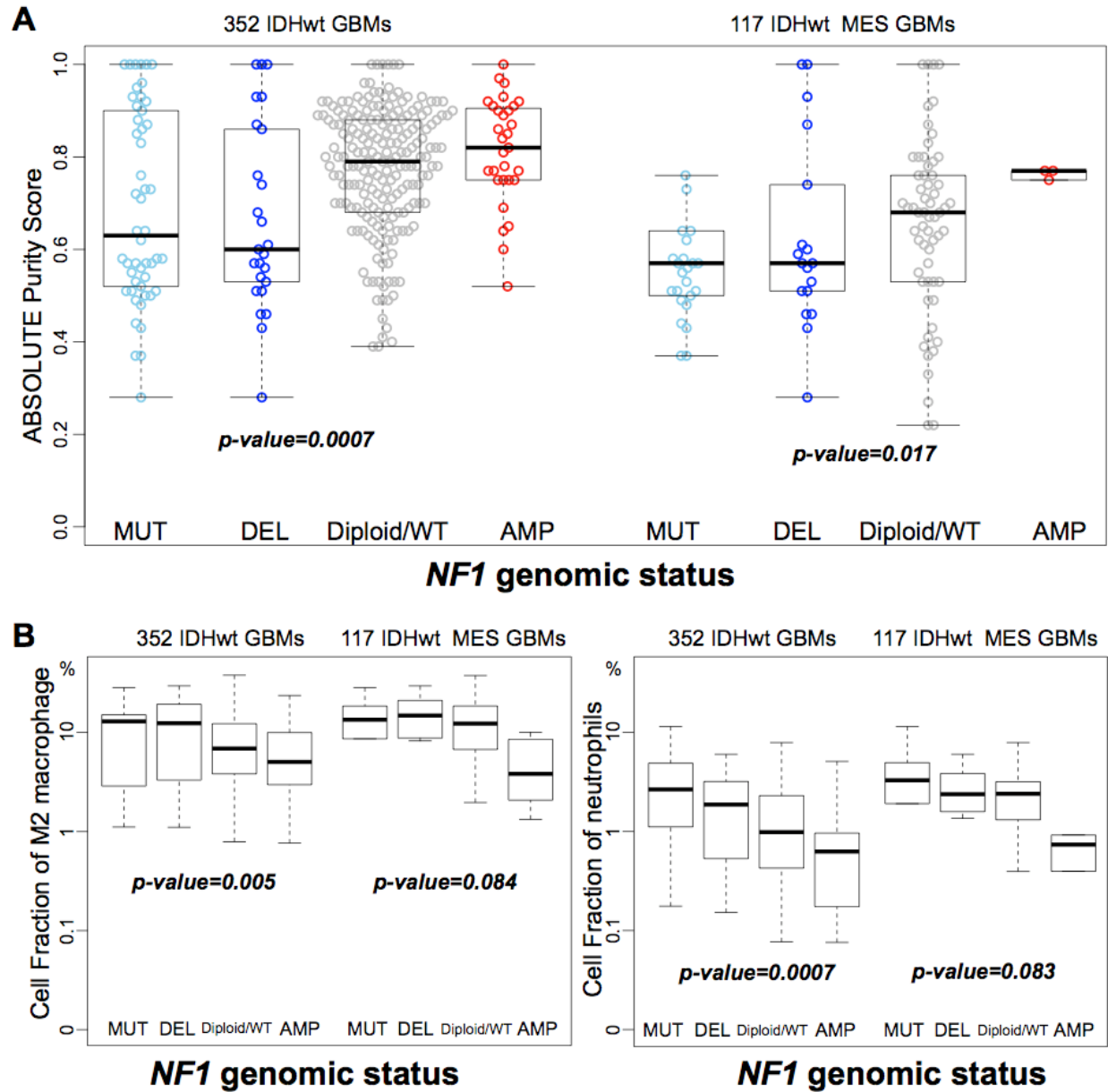
856
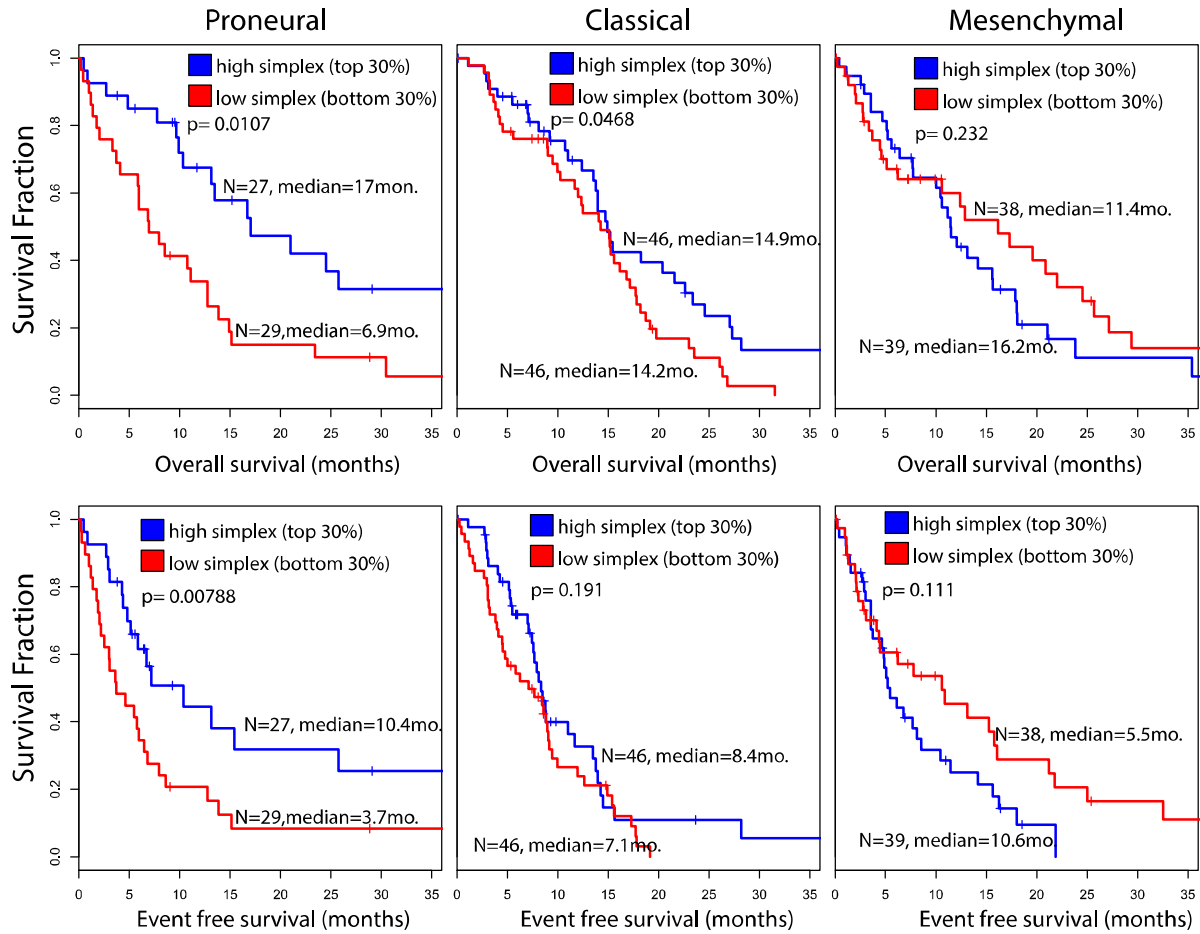
857

858　**Figure S5.** Overall and event free survival analysis comparison between samples with high and
859　low simplicity scores in each subtype.

860

Figure S6. Comparison of tumor purity and immune cell fraction between GBMs with different *NF1* genomic status. P-values were calculated using Wilcoxon rank test between samples carrying *NF1* deletion/mutation and others.
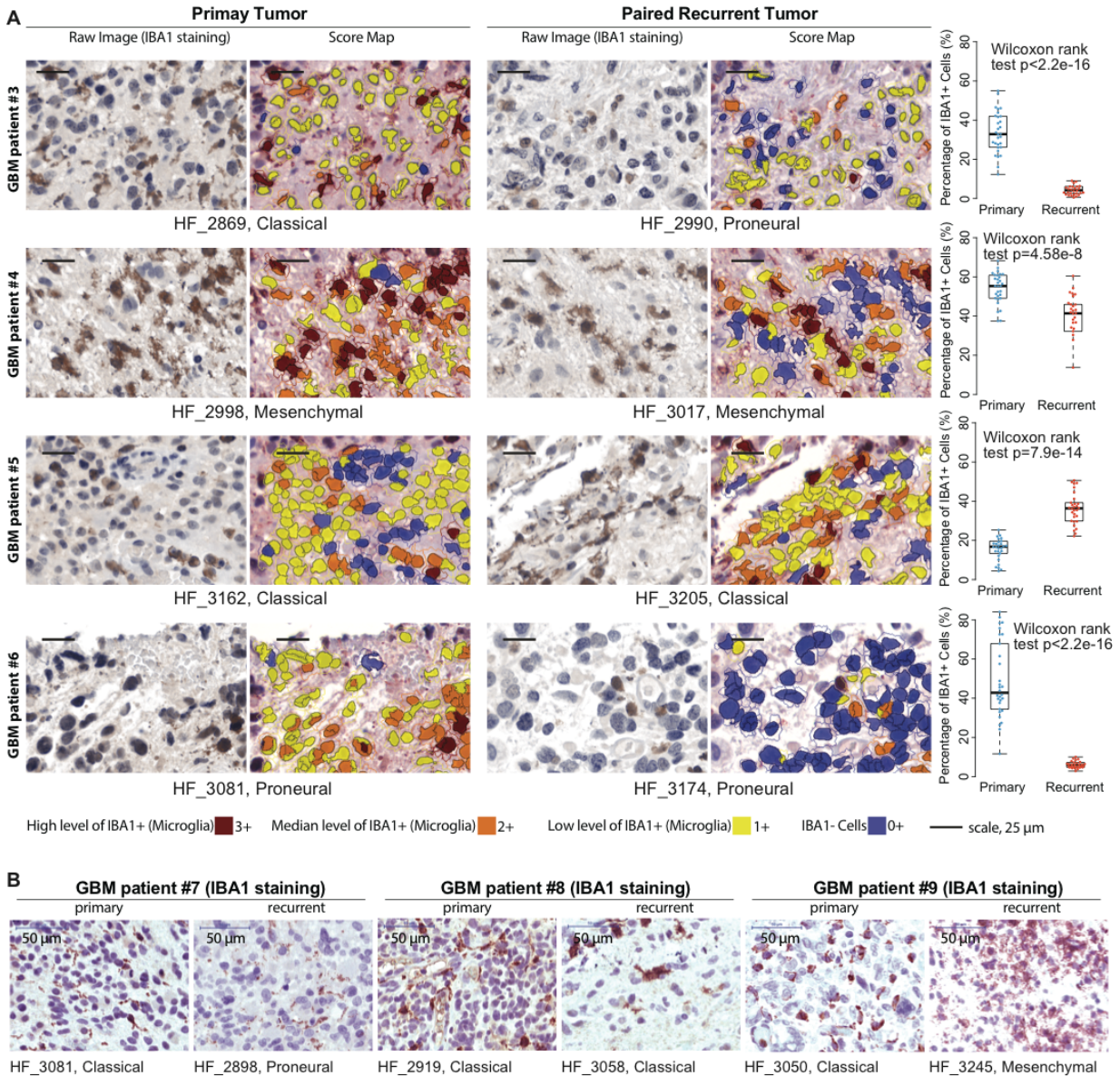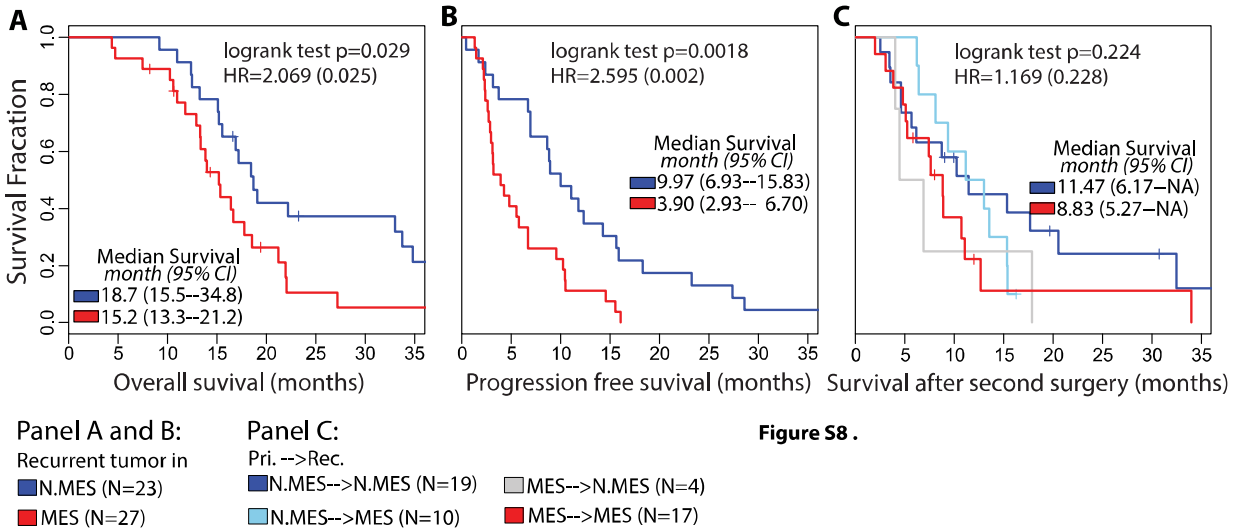
Figure S7. Immunohistochemistry staining of the IBA1 imcroglia marker. (**A**) Representative images with immunohistochemical staining of the IBA1 and score map obtained by InForm image analysis tools in four matched pairs of primary and recurrent GBM. Thirty scan fields were unbiased selected for each tumor by Calipar Vectra pathology imaging system automatically. (**B**) IHC staining of the IBA1 in three additional matched pairs of primary and recurrent GBM.

46

Panel A and B:
Recurrent tumor in
■ N.MES (N=23)
■ MES (N=27)

Panel C:
Pri. -->Rec.
■ N.MES-->N.MES (N=19)   ■ MES-->N.MES (N=4)
■ N.MES-->MES (N=10)   ■ MES-->MES (N=17)

Figure S8 .

875

876 **Figure S8. (A, B)** Overall and progression free survival analysis between samples in different
877 recurrent subtypes. **(C)** Survival after secondary surgery comparison between different
878 transition types.